PMUT and CMUT Devices for Biomedical Applications

A Review

Moisello, Elisabetta ; Novaresi, Lara ; Sarkar, Eshani; Malcovati, Piero ; Costa, Tiago L.; Bonizzoni, Edoardo

Important note
To cite this publication, please use the final published version (if applicable).
Please check the document version above.

TOPICAL REVIEW

PMUT and CMUT Devices for Biomedical Applications: A Review

ELISABETTA MOISELLO[1], (Member, IEEE),
LARA NOVARESI[1], (Graduate Student Member, IEEE),
ESHANI SARKAR[2], (Graduate Student Member, IEEE),
PIERO MALCOVATI[1], (Senior Member, IEEE),
TIAGO L. COSTA[2], (Senior Member, IEEE),
AND EDOARDO BONIZZONI[1], (Senior Member, IEEE)

[1]Department of Electrical, Computer and Biomedical Engineering, University of Pavia, 27100 Pavia, Italy
[2]Bioelectronics Section, Microelectronics Department, Delft University of Technology, 2628 CD Delft, The Netherlands

Corresponding author: Elisabetta Moisello (elisabetta.moisello@unipv.it)

ABSTRACT Piezoelectric Micromachined Ultrasonic Transducers (PMUT) and Capacitive Micromachined Ultrasonic Transducers (CMUT) have seen great developments in recent years, both in terms of performance and scope of applications within the biomedical ultrasound domain. This paper presents a review of the state-of-the-art of PMUT and CMUT technologies, focusing on their principle of operation, microfabrication techniques and use in different biomedical imaging and therapeutic applications. The advantages and drawbacks of PMUT and CMUT technologies in comparison with conventional bulk transducers are highlighted, the trade-offs among PMUTs and CMUTs are discussed, and their relevance in the current landscape of medical diagnostics and therapeutic uses is outlined, thus providing a clear overview of these promising technologies for the present and the next generation biomedical ultrasound applications.

INDEX TERMS PMUT, CMUT, ultrasound imaging, PAI, neuromodulation, biomedical.

I. INTRODUCTION

Ultrasound technologies are widely recognized for their significant role in advancing biomedical research and innovation. Their history of application goes back to the 1950s and their use in medical diagnostic imaging for visualizing fetal development during pregnancy [1], after which they developed as a general diagnostic imaging tool used in clinical practice. The emergence of ultrasound in the field of medical imaging was motivated by its favourable properties when imaging soft tissues, such as real-time operation, low-scattering, low absorption, lower-cost and portability, when compared to other imaging modalities, such as X-rays. In recent times, the field of biomedical ultrasound has witnessed advancements in imaging resolution for scanners (3D smart probes) as well as expansion to different medical applications, such as photoacoustic imaging (PAI), low-intensity focused ultrasound (LIFU) neuromodulation and

high-intensity focused ultrasound (HIFU) therapies. Furthermore, the form-factor of ultrasound probes has also been evolving from hand-held to wearable and even implantable devices.

A pivotal point for innovation in this field has been the growth of micro-electromechanical systems (MEMS) integration technologies, which present many opportunities as a valid alternative to advance ultrasound technologies beyond the traditional bulk transducers, both in terms of manufacturing and performance. On one hand, MEMS-based ultrasound transducer, such as Micromachined Ultrasonic Transducers (MUTs), benefit from compatibility with complementary metal-oxide-semiconductor (CMOS) technology, hence allowing for a manufacturing process with lower cost, higher design flexibility and reproducibility; indeed they support MEMS-CMOS integration on the same package, which is a fundamental aspect to reduce the parasitic elements, size, weight, and power consumption of the overall system [2]. On the other hand, Capacitive-based MUT (CMUT) and Piezoelectric-based MUT (PMUT), the two

The associate editor coordinating the review of this manuscript and approving it for publication was Riccardo Carotenuto.

primary technologies in this domain, are able to overcome many performance limitations given by bulk transducers, specifically in terms of frequency of operation [3] and acoustic impedance matching to biological tissues [4]. Given these properties, MUT devices feature a wide range of applications, not only limited to the biomedical field, but also including physical sensors for assessing fluid properties (e.g. viscosity, density, and flow velocity) [5], [6], [7], [8], humidity sensors [9], eye tracking [10], particle manipulation [11], chemical and gas detection [12], structural health monitoring [13], [14] and airborne applications such as gesture recognition and haptic feedback [15].

Since research nowadays is heavily focused on PMUT and CMUT innovation for biomedical applications, this paper will provide a literature review focused specifically on the biomedical field, aiming to analyze in detail the state-of-the-art and highlighting the CMUT and PMUT advantages and disadvantages, and eventually draw a comparison between the two, concerning their use in medical applications.

The paper is organized as follows. Section II illustrates the MUTs principle of operation, Section III details their fabrication steps and employed materials, Section IV provides the state-of-the-art overview on biomedical applications, considering the specific cases of medical imaging, photo-acoustic imaging, ultrasound-based therapy, implantable devices and other medical applications such as wearable devices and inhalation therapy, and Section V concludes the paper by providing a comparison between PMUT and CMUT, while highlighting the current preferences in the medical field as well as possible future developments.

II. MUTS PRINCIPLE OF OPERATION

Medical ultrasound is generally addressed as the exploitation of electro-acoustic signals in the range of hundreds of kHz to MHz for diagnostic or therapeutic applications. In this context, for an electrical signal to get converted into acoustic signal and vice-versa, transducers in the form of transmitters and receivers are required: specifically, CMUT and PMUT behaving as actuators and/or sensors and featuring a membrane which vibrates in a flexural mode, can be employed. To describe how these devices work in the mechanical domain, the mass-spring-damper model, illustrated in Fig. 1(a), is presented. Assuming the flexion of the membrane of the MUT as a piston-like movement of a rigid plate of mass m, when a force is applied to the membrane, it flexes with an opposite force and restores the equilibrium: this effect can be modeled by a spring with elastic coefficient k. All the energy losses, including the acoustic-mechanic coupling losses, can be modeled as a damper with damping coefficient b. Applying Newton's second law, a second order differential equation which describes the MUT flexural movement of the membrane can be derived

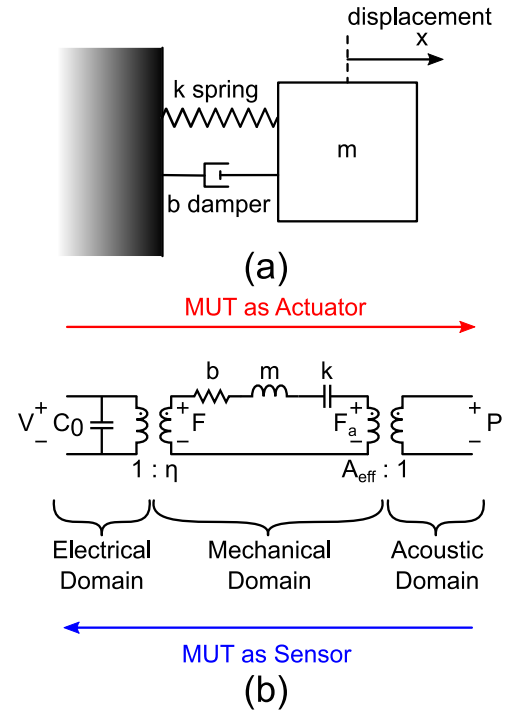$$m \frac{d^2x}{dt^2} + b \frac{dx}{dt} + k\,x = F \tag{1}$$

FIGURE 1. (a) Spring-mass model and (b) simplified Mason model.

where x is the flexural displacement of the MUT membrane, and F is the resultant force applied to the membrane, considering the acoustic force, the electrostatic force or the force due to the piezoelectric effect (if present) and the impact of the ambient pressure. From the second order differential equation it is then possible to derive the MUT resonant frequency.

Although the mass-spring-model correctly summarizes the membrane flexural movement, it doesn't permit the estimation of the MUT's electrical properties, which are vital for examining and designing the transducer's front-end electronics. For this reason the equivalent circuit model, known as Mason model, illustrated in Fig. 1(b), is introduced. It models the electro-mechanical-acoustic operation of the transducer, linearized around a bias point [16], [17], not considering non-linear distortion effects. Nevertheless, it provides a strong basis to approximate MUTs performance, enabling to predict the electrical and mechanical losses, as well as the transducer-medium interactions where the values of the equivalent inductor, capacitor and resistor are paired to the mass, spring and damper of the mechanical model, respectively. The Mason model is the same for the transducer acting as actuator (Transmitter, TX mode) or sensor (Receiver, RX mode). In the electrical domain a voltage V is either applied on or sensed by the MUT depending on their behavior as actuator (transmitter) or sensor (receiver) respectively, while C_0 represents the static capacitance of the transducer. The electrical domain is converted into the mechanical domain through an ideal transformer of ratio $1{:}\eta$, where η is the electro-mechanical coupling coefficient, while

the mechanical domain is converted into the acoustic domain by means of an ideal transformer with a ratio equal to A_{eff} :1, where A_{eff} is the area of the transducer membrane. In this way, the voltage V is transformed into force F and force F is converted into acoustic pressure P.

The illustrated mass-spring-damper and Mason models are effective for studying the MUTs principle of operation, however, they entail notable simplifications without accounting for all the non-linear behaviors and general non-idealities in the device. Hence, in order to appropriately design and characterize the MUT devices, the finite element method (FEM) analysis, both static and dynamic, can be used to study their almost accurate behavioral properties [5].

In the following subsections, the physics behind PMUTs and CMUTs are described more in detail, focusing especially on their behaviors relevant to biomedical applications.

A. PMUT

Traditionally, the most basic physical mechanism to produce ultrasonic signals are either piezoelectric effect, magnetostriction or the photo-acoustic effect [18]. The piezoelectric effect in particular is exploited in PMUT, as well as in conventional bulk PZT transducers, and it is defined as the property of certain materials (such as piezoceramics or crystals) to physically deform in the presence of an electric field or, conversely, to generate an electrical charge when mechanically deformed [3]. To describe this phenomenon, the canonical equations of piezoelectricity are introduced:

$$S = [s^E]T + [d^T]E \qquad (2)$$

and

$$D = [d^E]T + [\varepsilon^T]E \qquad (3)$$

where S and T are, respectively, the strain and stress tensor, E and D represent the electrical field and the charge density vector, $[s]$ is the matrix of compliance constants $[\frac{m^2}{N}]$, $[\varepsilon]$ is the permittivity matrix $[\frac{F}{m}]$, and $[d]$ is the matrix of piezoelectric coefficients $[\frac{C}{N}]$. Among these coefficients, the PMUT working principle is based on the flexural vibrations caused either by d_{31} or d_{33} mode excitation of a membrane (where d_{31} and d_{33} represent, respectively, lateral and perpendicular contraction/expansion of the material due to an applied voltage). These vibrational modes are responsible for the generation of ultrasound mechanical waves in the presence of an input voltage and vice-versa.

In order to express a measure of the effectiveness of the electromechanical coupling and, thus, of the effectiveness of the device itself, the Electromechanical Coupling Coefficient (EMCC) can be considered as metric [19], [20].

In Fig. 2 a general schematic of a PMUT transducer is presented. The device is composed of a piezoelectric film, ranging in thickness from hundreds of nanometers to a micrometer, sandwiched between two electrodes—top and bottom. Below this, a passive layer of Silicon dioxide (SiO$_2$) of tens of micrometers, provides support to
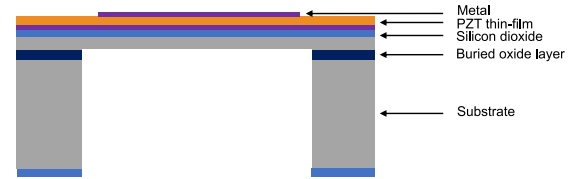

FIGURE 2. PMUT cross section schematic.

the piezoelectric thin-film during its transduction process; furthermore, it changes the natural axes of the membrane, thus translating the lateral stress (produced by the d_{31} mode) to a deformation of the membrane out of plane which enables actuation of the membrane in its flexural modes. Beneath the structure lies a cavity, which is integral to the device resonance principle. Its dimension is specifically designed to align with the resonant frequency of the piezoelectric thin-film membrane.

The resonant frequencies of the PMUT depend on the shape, dimensions, boundary conditions, intrinsic stress and mechanical stiffness of the membrane [21]. The most commonly reported diaphragm shapes in reported literature are circular and square. These shapes are favored due to their consistent reliability and the simplicity they offer for equivalent modeling, given that their resonant frequencies can be determined analytically [15]. In particular, for a circular-shaped fully-clamped transducer, the resonant frequency is given by:

$$f_r = \frac{\alpha}{2\pi r^2}\sqrt{\frac{D_E}{\rho h}} \qquad (4)$$

where α is the first mode circular constant, r is the membrane radius, D_E is the flexural rigidity, ρ is the membrane density, and h is the membrane thickness. In [22] the effect of electrode design on the performance of the PMUT is discussed in detail.

Recently, there has been some published works that feature more peculiar shapes for the membrane, such as piston-like [23], island-shape [24], I-shaped [25], bimorph [26] and pre-concaved [27]. Starting from the piston-shape structure [23], the device is a squared PMUT with four symmetric rectangular openings, on each side, thus creating a "tent-plate" shape. The passivation layer seals the openings, thereby enlarging the movement of the membrane while making it liquid-proof, so that it is able to work in a liquid environment as well. This eliminates the limitations of clamped boundary used in regular PMUT devices, making it undergo larger displacement as compared to the clamped PMUTs. Consequently, the paper reports an increase in the output acoustic pressure by using this proposed device. The study presented in [24] overcomes the issue of mechanical fractures in traditional PMUT designs by enhancing the supported diaphragm displacement thanks to the employment of an island-shaped structure with a ring-shaped polyimide thin film. This provides excellent mechanical flexibility of the device because of its higher elasticity, and hence
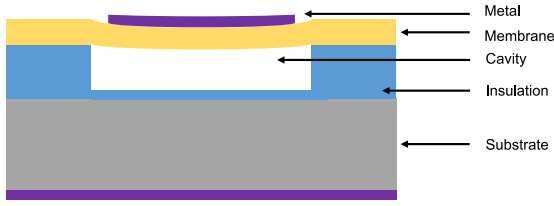
FIGURE 3. CMUT cross section schematic.

larger displacement of the membrane. An I-shaped composite diaphragm [25] was developed to improve the sensitivity and resonant frequency of PMUTs with the same diaphragm area as compared to square and circular diaphragm of PMUTs. Instead, [26] proposed a two active layers ("bimorph") structure, with opposite electric fields in the two active layers due to the electrode configurations. This induces opposites stresses in each of the piezoelectric layers, thereby generating four times the bending moment as compared to the regular "unimorph" PMUT when the middle electrode is driven differentially, but the top and bottom electrodes are grounded. This proposed device also shows higher displacements per input voltage at particular resonant frequencies, four times high driving sensitivity and high energy-efficiency in comparison to state-of-the-art PMUTs with similar geometry and frequency. Lastly, [27] presents a pre-concaved membrane which is beneficial for piezoelectric coupling. It offers a low impedance, high quality factor and large displacement performance in air coupling that can be used in high frequency application such as medical ultrasonic field.

B. CMUT

Part of the micromachined ultrasound transducer category, CMUTs rely on the electrostatic transduction mechanism. The vibrating membrane of a CMUT, includes a conductive layer which acts as a top electrode. The bottom electrode is usually represented by the conductive substrate. Between the two, a cavity is present, inside which an electric field is generated when a voltage is applied to the electrodes. The vibrating membrane is commonly designed in squared, circular, or hexagonal shapes [28], [29], [30]. This membrane is anchored at its periphery and is suspended over the cavity. The cavity can be vacuum or air filled and typically features an electric field of the order of several tens of volts per μm or higher, thus resulting in a high electromechanical coupling coefficient [5]. In order to prevent any contact, and consequent short circuit between the electrodes, an insulating layer is also added. A schematic representation of a generic CMUT cross section is illustrated in Fig. 3.

The CMUT, therefore, in a first order approximation, acts as a parallel-plate capacitor with a moving top electrode. In order to generate acoustic pressure waves, the diaphragm can be actuated by the electrostatic force,

$$F_e = \frac{-A\epsilon_0\epsilon_r V^2}{2(g_{eff} - x)^2} \tag{5}$$

where A the top electrode area, ϵ_0 the vacuum permittivity, ϵ_r the relative permittivity of the insulator and membrane material (assumed to be the same), V is the voltage applied to the capacitor plates, x the top electrode displacement, $g_{eff} = (t_i + t_m)/\epsilon_r + g_0$ is the effective gap height, g_0 the initial gap distance under V equal to zero and with no stress applied, t_i the insulator thickness and t_m the membrane thickness. In this way, by changing appropriately V, the generated time-varying electrostatic force causes the diaphragm to vibrate, thus creating ultrasound waves [31]. When working as sensing element, acoustic waves cause the membrane to vibrate, resulting in a capacitance variation, which in turn is converted into a variable voltage and/or current under electrical biasing of the CMUT [5]. Assuming a membrane displacement equal to x and a vacuum cavity, the capacitance of the equivalent parallel-plate capacitor is given by [31]

$$C = \frac{A\epsilon_0\epsilon_r}{g_{eff} - x} \tag{6}$$

The CMUT operation, both as actuator and as sensor, can be studied according to the second order differential equation derived relying on Newton's second law and the electromechanical model reported in Section II. The obtained equation is non-linear in the displacement x; for most applications, however, the CMUT is biased with a large DC voltage (V_{DC}) and then modulated through a small AC voltage (V_{AC}), resulting in overall voltage $V = V_{DC} + V_{AC}$, in the actuating mode or an acoustic pressure in the sensing mode. Hence, the linearization of the electrostatic force becomes a function of DC bias [31].

Concerning the DC bias voltage, when it is applied on the top electrode, the electric field causes it be displaced more and hence the top electrode displaces further, showing the phenomena of spring motion. However, if the DC bias voltage is increased beyond a certain value, the diaphragm collapses onto the bottom electrode, i.e. the displacement of the top electrode can result in an increase in the electric field to the point where the attractive electrostatic force overcomes the diaphragm stiffening force [32]. The critical bias voltage for which the collapse phenomenon occurs, known as pull-in voltage, is

$$V_{collapse} = \sqrt{\frac{8k_p g_{eff}^3}{27\epsilon_0\epsilon_r A}} \tag{7}$$

where k_p is the spring constant of the equivalent mass-spring model [31].

Although conventionally the collapse mode is avoided, as it suffers from non-linearities, it can be beneficial since it allows achieving higher output pressure and electromechanical coupling efficiency with respect to the conventional mode [32]. There are different variations of collapse mode: traditional collapse mode, collapse snap-back mode and deep collapse mode [32]. In traditional collapse mode the central part of the diaphragm is in contact with the substrate, in collapse snap-back mode the CMUT is first set in collapse state and then the membrane is allowed to lose contact with the substrate

by adjusting the applied voltage, whereas in deep collapse mode the applied AC voltage is larger than the collapse voltage. Depending on the desired transducer characteristics and performance, therefore, the most appropriate operating mode must be chosen.

III. MUTS FABRICATION STEPS AND MATERIALS

In this Section an overview on the state-of-the-art materials and methods employed for the integration of MUTs is presented.

A. PMUT

For what concerns the materials exploited to fabricate the piezo layer, there are different options which can be divided into two main categories: lead-based thin film and lead-free thin film [15]. The most prominent member of the first category is PZT (Lead Zirconate Titanate), either monocrystalline or polycrystalline. PZT is a piezoelectric material developed for the first time in 1952 and it is the most common option for PMUT membrane because of its high piezoelectric constant d_{31} (ranging from $80\frac{pC}{N}$ to $130\frac{pC}{N}$), making it a suitable candidate for medical ultrasound for its high sensitivity with low input voltages. The thin-film PZTs are developed either through a physical approach (e.g. RF/laser sputtering) or by chemical coating technique (e.g. MOCVD, sol-gel). Sol-gel in particular is widely popular to grow PMUT membranes since it easily allows depositing PZT films with good properties in a thicknesses range varied up to 1 micron with high uniformity features [33]. The idea behind it is to coat the PZT solution, which is a mixture of precursors and agents, by dipping or spinning the wafer. Then, the wafer is sintered, increasing the temperature from 600°C to 700°C. In this way, the PZT will be crystallized and the solvent will be released [34]. The downside of the sol-gel technique is the heating associated with it, which can cause cracks and delaminations.

The cavity of the PMUT must be formed with either front-side etching [35], backside etching [36] or sacrificial layer release [37]. In the first technique, the cavity is defined by etching the front side of the membrane via a hole in the piezoelectric layer. This allows for a better resolution in the definition of the substrate cavity but implies a further process step in order to eventually seal the hole which can alter the functioning of the device. Backside etching on the other hand means that the cavity is formed by etching the substrate from the backside. This passage happens either before or after the deposition of the PZT membrane and, in order to obtain well-defined vertical walls of the cavity, deep reactive ion etching (DRIE) is commonly used [38]. Lastly, the third technique involves the initial preparation of a sacrificial layer on the substrate. After completing the rest of the fabrication, this layer is then released by wet-etching through a small opening in order to form a cavity. Its main advantage is that it allows the formation of small cavities, however, in some
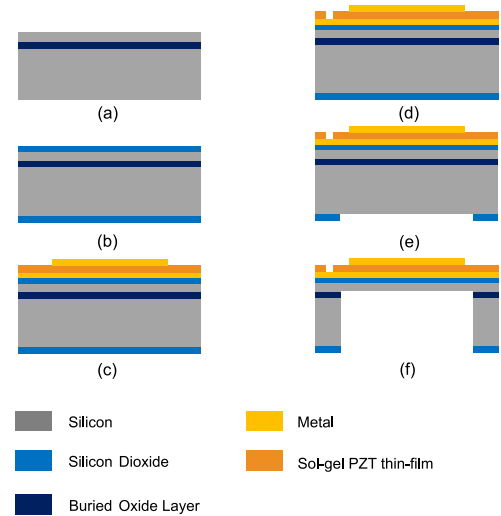
FIGURE 4. Fabrications steps of PZT PMUT with sol-gel and back-side etching.

cases, stiction of the membrane to the substrate can occur, which could, potentially damage the structure.

In Fig. 4, an example of fabrication stages of a PZT-based PMUT is presented, featuring sol-gel and backside etching: The process begins with showcasing an SOI (silicon on insulator) wafer (a). Following this, both sides of the wafer undergo a thermal deposition of silicon dioxide (b). On the top of the SOI wafer, a metal, typically Ti/Pt, is sputtered, serving as the bottom electrode. Subsequently, PZT is deposited using the sol-gel method. Post optical lithography patterning to define top electrode, another metal layer, usually Cr/Au, is sputtered (c). A section of the PZT is wet-etched, ensuring access to the bottom (ground) electrode (d). Deep-reactive ion etching (DRIE) is then carried out on the SOI wafer's bulk Silicon from the bottom, following a backside alignment (e). The process culminates with reactive ion etching (RIE) targeting the buried silicon dioxide of the SOI wafer (f). Importantly, the silicon layer beneath the metallized thin-film PZT acts as a safeguard, ensuring the membrane remains intact during PMUT transduction.

Even though bulk ceramic PZT shows high piezoelectric constants, its use is rather limited in PMUT fabrication due to the difficulty of thinning the membrane below 50 μm, but in [39] a new process for scaling ceramic PZT down to 5 μm using CMP (chemical mechanical polishing) is reported. This method would significantly improve the performance of the MEMS device at high frequency.

As previously mentioned, lead-free materials can be employed in PMUT designs in order to solve health hazards coming from the handling of lead materials in the PZT integration process: the most important player in this category is AlN (Aluminum Nitride), which, even though presents a lower d_{31} factor with respect to PZT ($2/5\frac{pC}{N}$), requires lower temperatures during fabrication (usually completed through sputtering) and has good CMOS compatibility.

In [40], a multi-element ring ultrasound transducer array is presented which is based on AlN PMUTs and eliminates the dependence of acoustic wave frequency on the diameters of the annular array, achieving accurate control of the focus depth; in [41], an AlN corrugated diaphragm is realized with no additional steps in the work flow in order to improve the volume up to $3.2\times$ higher than the conventional PMUTs. The process allows for a high fill-factor (80%) array PMUT with high resonance frequencies. Scandium doping is often used to increase the dielectric constant of pure aluminum nitride (ScAlN with 15% dosage in [42] and 36% in [43]) while maintaining process compatibility with existing AlN based manufacturing. This allows an increase in the transmit amplitude, consistent with an increase in the transverse piezoelectric coefficient. Scandium alloyed [44] (AlScN) has also been investigated as an alternative to ScAlN because of its unique advantages, such as its strong piezoelectric effect and high thermal stability, even though it presents many challenges during fabrication.

Other less popular lead-free solutions for PMUT piezo layers include $LiNbO_3$ (Lithium Niobate) [45], PVDF (Polyvinylidene Fluoride) [46] and ZnO (Zinc Oxide) [47].

Regarding flexible PMUTs, they have been extensively studied recently due to their numerous potential medical uses, such as brain stimulation and non-invasive diagnostics: one possible method of integration is the use of a flexible substrate, so that the main factor that influences the fragility of the device is the thickness of the piezoelectric film. In [48], fabrication of flexible PMUTs using flexMEMS technology is described, where the PMUTs were developed on flexible polyimide substrates instead of the conventional rigid silicon substrate. In [49], the bendable structure is made out of several silicon islands containing a PMUT PZT array and are connected to each other by silicon springs, resulting in a fully conformal silicon based structure without the necessity of thinning down the wafer.

An interesting innovation in biomedical diagnostics is the so-called super-harmonic imaging, which is a beneficial extension to the fundamental imaging by exploiting the third-to-fifth harmonics: this becomes a challenge for the development of ultrasonic transducers in terms of bandwidth. For this reason, in [50] in order for the PMUT array to have two different resonance frequencies, the possibility of suppressing the in-band spurious structure by controlling the piezoelectric polarization direction was studied. As a result, it was found that the spurious structure between the resonance frequencies can be relaxed and the bandwidth can be expanded by controlling the polarization direction. To overcome assembling limitations of two types of transducers in the same array, in [51] dual frequency PMUT were developed utilizing the first two natural vibration modes of their single PZT diaphragm by setting up two top electrodes. In [52], a multi-frequency flexible array has been developed using a polymeric PVDF layer. This proposed PMUT array, rather than incorporating numerous single-frequency transducers, has demonstrated the ability to
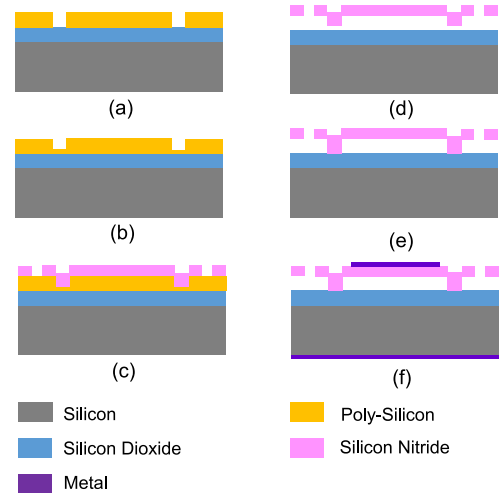

FIGURE 5. CMUT sacrificial release fabrication process.
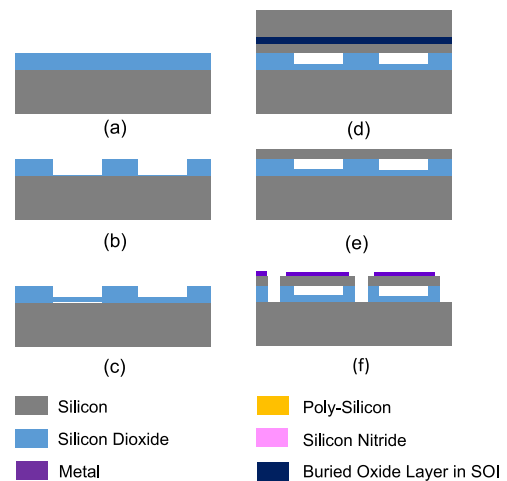
FIGURE 6. CMUT wafer bonding fabrication process.

operate at multiple frequencies, achieving a penetration depth of 63 mm. This shows promise for facilitating multi-scale harmonic imaging in a compact and portable format.

B. CMUT

The fabrication process flow of CMUTs involves several steps: material deposition, lithography, etching. The choice of the silicon wafer and its surface condition significantly affects the CMUT devices mechanical and electrical properties. Most commonly, two types of fabrication methods are employed: sacrificial release process or wafer bonding [5], [31].

The sacrificial release process, based on surface micromachining, allows creating the CMUT cavity by etching a sacrificial layer between the top plate and the substrate [5], [31]. The process steps are schematically illustrated in Fig. 5. Firstly an insulator layer (silicon nitride or silicon dioxide, which also acts as an etch-stop layer) is deposited on the silicon substrate and bottom electrode, represented by

the conventional conductive silicon substrate, after which a sacrificial layer (typically polysilicon) is deposited and patterned to define the post area between cells (a). Then a second sacrificial layer is deposited, in order to create the etching channels into the cell (b). The combined thickness of the two sacrificial layers determines the cavity height. Next the membrane structural layer is deposited above the sacrificial layer and adequately patterned, in order to define the etch vias, i.e. the holes made in the top layer in order to access the sacrificial layer and the etching channels (c). Subsequently the sacrificial layer is etched (d), typically employing a potassium hydroxide (KOH) wet etch, thus releasing the membrane and forming the CMUT cavity. The cavity, however, is vented to the atmosphere from the gaps corresponding to the etch channels: hence, the etch vias are sealed with a suitable technique (e), e.g. low-pressure chemical vapour deposition (LPCVD), which allows to effectively vacuum-fill the cavity when it is sealed. Vacuum is preferred as it allows reducing energy losses; when the CMUT works in air, it suffers from compressed gas damping of the cavity, while when it works in a liquid environment it suffers from hydrolyzation caused by the strong electric field in the cavity: vacuum sealing of the cavity can reduce both these types of losses [53]. Finally the top and bottom electrode are formed by depositing and patterning an appropriate metal (usually aluminum) on the top plate and the substrate (f). The whole CMUT cell can then be protected by a sealant in order to prevent a performance degradation in the device. The sacrificial release process is simple and reliable, provides good yield and can be designed in order to be used at a low maximum processing temperature (250°C), thus allowing postprocess CMOS integration; however, it suffers from intrinsic stress in the membrane material and limits in the membrane thickness and cavity height, which alter the device properties and performance [31].

Wafer bonding techniques consist of a combination of surface micromachining and silicon-on-insulator (SOI) technologies, which allows developing the membrane and the cavity in two separate wafers [5], thus enabling optimization of both the membrane and cavity simultaneously [54]. There exist different wafer bonding techniques which are commonly used: fusion bonding, anodic bonding, and adhesive bonding.

A basic CMUT fabrication process flow through wafer bonding is illustrated in Fig. 6. The starting point is a heavily-doped silicon wafer with an insulation layer, typically in silicon oxide, on the top (a). The insulation layer is then etched in order to define the CMUT cavity (b): hence, the cavity height is determined by the insulating layer thickness. The cavity is realized directly in the insulating material as it allows reducing the effect of parasitic capacitances. A thin electrical insulation layer is then added in order to passivate the exposed silicon substrate and ultimately avoid shorting between the top and bottom electrodes (c). A second wafer, typically an SOI wafer, is bonded onto the

cavity (d): the bonding is performed so that the device layer of the SOI wafer faces the cavity side of the first wafer. The bonding is usually performed in vacuum in order to create a vacuum-filled cavity [55], as it is obtained with the sacrificial release process. The CMUT membrane is then formed by etching the handle wafer and the buried oxide (BOX) layer of the SOI wafer (e): hence the membrane thickness corresponds to the device layer of the SOI. Since SOI wafers can be manufactured with a wide range of highly uniform device layer thickness, a wide range of CMUT membrane thickness can be supported. Finally metallization for creating the electrodes and low-temperature passivation complete the process (f).

Compared to the sacrificial layer process, wafer bonding techniques ensure better control over the membrane thickness and cavity height and lower residual stress; however, the wafer bonding step itself constitutes a drawback as its yield, decided by the cleanliness and smoothness of the surface, is typically low. An additional drawback is given by the cost and logistical complexity of procuring suitable SOI wafers: to avoid this, silicon nitride can be deposited on a standard wafer and bonded to the substrate wafer from the top plate [31]. Conventional wafer bonding technology requires high temperatures (more than 1000°C) to ensure good bonding quality [56], which constitutes another drawback as it prevents integration of CMUTs [54]; moreover, a high temperature could result in the degradation of thermally sensitive devices and residual stress in processed silicon wafers with different thermal expansion coefficients. However, methods for fabricating CMUTs with low-temperature wafer bonding at 400°C have been developed by activating the surfaces by creating more hydroxyl (OH) groups, which results in higher hydrophlilicity [57]. Surface activation can be achieved by treating the SOI wafer and the substrate with oxygen plasma or wet chemical or both, however treating the pre-bonded wafers to chemicals containing various reagents to activate their surface, followed by O_2 plasma treatment helped to improve the hydrophilicity [57]. Alternatively, also anodic bonding enables CMUT fabrication with low thermal budgets; furthermore, it can also improve the CMUT transparency, thus allowing coupling with optical measurement techniques [31]. Another issue in CMUT wafer bonding fabrication can be the pre-charge due to charge trapping and ion drift in the insulating layer within the gap, which can determine a hysteresis in the electrostatic deflection of the plate. In order to avoid the pre-charging issue, thick BOX layer SOI wafers or tailoring of the insulating layer dielectric constant can be employed [28], [31]. Pre-charging can also be exploited to electrostatically deflect the CMUT plate, thus reducing or entirely removing the DC pull in voltage [31].

In recent years, in addition to the standard sacrificial release and wafer bonding processes, polymer-based CMUT microfabrication approaches have also been proposed, as they enable the realization of flexible devices, which can solve

the challenge of transducer operation on non-planar surfaces [58], [59], [60].

Although typical ultrasound transducers operate in a defined frequency band, primarily determined by the size and thickness of the membrane, the need for multi-frequency transducers is emerging for different applications, including multi-scale imaging, image-guided HIFU and contrast imaging [61]. In CMUTs, a possibility to support multi-frequency operation is employing different modes (conventional and collapse) and tuning the bias voltage across the membrane [62], [63]: indeed, due to the spring softening effect, the CMUT resonance frequency shifts to lower values by increasing the applied bias voltage. Another approach, proposed in [61], exploits the fact that CMUT membranes can be made smaller than the generated acoustic wavelength in order to create dual frequency arrays where large and small membranes are interlaced on a scale smaller than the operating wavelengths: in this way deep penetrations with low resolution and higher resolution at shallow imaging depth can be simultaneously supported by the same transducer, thus enabling multi-scale imaging.

IV. PMUT AND CMUT FOR BIOMEDICAL APPLICATIONS

In this Section the most prominent case studies of biomedical applications featuring PMUTs and CMUTs that have been published in the last few years are presented, including some recent in vivo experiments.

A. ULTRASOUND IMAGING

Historically, diagnostic imaging (ultrasonography) has been the main application of ultrasound technologies in the biomedical field. An image of the internal organs is created using the reflected echo signals from transmitted ultrasound acoustic waves (TX) when they interact with a medium. These transmitted waves, produced by a transducer probe (acting as a transmitter) attached to the patient's body, travel inside the body. As they encounter tissues of varying acoustic impedances, they undergo attenuation, reflection, and refraction, resulting in the generation of reflected echoes that form the image. The probe is also used in reception (RX) mode, acting as a receiver to sense these echoes. Usually the probe contains not one single transducer, but an array of them: in TX mode, the employed electronics sets the time or phase delay with which the excitation pulses, either short burst pulses or continuous waves, make the transducer steer and focus the beam in a different direction and depth, which helps to scan the whole organ section. 3D volumetric images are possible when the probes are made as a 2D matrix of mini-transducers instead of just a linear array [64]. PMUT and CMUT specifically offer an interesting alternative with respect to traditional bulk PZT-based transducers due to their ease in fabricating interconnections for highly densed arrays. Since traditionally ultrasound imagers relied on piezo-based transducers, PMUT represented the natural evolution for new generation probes, however, in recent years the focus

has shifted towards CMUT-based solutions for this specific imaging application.

CMUTs main advantages with respect to PMUTs in this field include their wide bandwidth, although both PMUT and CMUT offers low-cost manufacturing and the possibility to integrate the transducer monolithically on top of ASIC via flip-chip bonding [65], [66]. Moreover, CMUT cells can be easily fabricated and arranged in arrays (thus enabling 3D ultrasonic imaging [66]) and show high directivity and beam steering capability with wide working temperature range.

In order to improve the CMUT performances in ultrasound imaging, the research has focused on the investigation on both the single cell and the array structures. A novel array structure consisting of additional flexible moving membranes besides the regular one, suspended between the transducer top membrane and the fixed bottom electrode was presented in [66]. The presence of the additional middle membrane increases the membrane displacement amplitude, and hence the effective cavity height decreases, so the pull-in voltage reduces, as seen from equation (7), while the transducer acoustic output power and sensitivity are enhanced, showing promises for high performance imaging applications. Non-uniform membranes [67], interlayer metal structures [68] or a combination of the two [69] were also employed for improving the transducer performance: non-uniform top membranes lead to softened film structures, which increase the CMUT dynamic range and bandwidth, while interlayer metal structures enhance sensitivity as they enable the realization of narrow spaces between top and bottom electrodes. By combining multiple CMUT cells in array structures, super-resolution and 3D imaging can be implemented. The main challenge in array design is the number of required interconnections: by employing a row-column addressed scheme to a N×N matrix, the required interconnections are only 2N, while N^2 interconnections are needed if a conventional fully populated matrix scheme is used [70]. As the resolution capability is directly proportional to N, CMUT arrays with high number of channels are required. Zig-zag patterns can be adopted in CMUT array design in order to increase the active area of the cells for a fixed plate thickness [70]. Rectangular [66], annular [71], [72] and spiral [30] shapes can be realized through the flexibility in CMUT array fabrication.

On the other side, recent examples of PMUT employment for ultrasound imaging purposes include [73], a 2D array based on a strongly c-axis-oriented AlN thin film having a 2.82 MHz resonant frequency. Miniaturized PMUTs (N = 400, each 40 μm in radius) were integrated into a 2 × 2 mm^2 area and displayed a high fill factor of 50.27%. This PMUT array shows great promise for portable and implantable imaging applications, owing to their low sinusoidal input (10 V, as reported) in contrast to CMUT which requires high DC bias voltage (> 100 V). In [74] a 64 element 1-D PMUT array for low-frequency diagnostic imaging applications is presented, showing peak transmit and receive sensitivities assessed at the transducer surface equal

to 31 kPa/V and 3.2 mV/kPa respectively. The experimental setup used for the imaging tests includes in vitro sector scan of a portion of the phantom and in vivo linear scan of a human carotid artery. In [75], high frequency (6 MHz) and low frequency (1.5 MHz) PMUT arrays with 128 channels for medical imaging applications are proposed. In particular, the proposed high frequency array has a transmission sensitivity of 45 kPa/V at 3-cm distance and a receive sensitivity of 204 mV/MPa. The high transmission sensitivity is also beneficial in having a high depth of penetration and obtaining high resolution images. The functionality of the transducer arrays is confirmed by obtaining B-mode images in water medium.

For breast monitoring applications, [76] presents a multi-perspective ultrasound imaging technology with the cylindrical motion of four 128 elements PMUT rotatable linear arrays (featuring 3.5 MHz resonant frequencies) with 90 degrees to each other, which allows for non-invasive detection. A breast model with a 2-cm mass in the center and six 1-cm superficial masses were used for the experimental analysis. Combined with ultrasound imaging algorithms, multi-perspective ultrasound imaging was realized including vertical slices, horizontal slices and 3D imaging. The seven masses were detected and the absolute error of the size was approximately 1 mm where even the image of the injection pinhole could be seen.

Multi-frequency operation is required in acoustic angiography applications, where a focused low-frequency ultrasound beam is used at the transmitter side to excite the contrast agents, known as microbubbles, injected in the bloodstream, while sensing of high frequencies (third and higher harmonics) is targeted at the receiver side for eliminating unwanted reflections in the surrounding tissue and instead imaging only the microbubbles [77]. The different response of tissue (linear) and microbubbles (highly non-linear) to acoustic excitations allows generating images with high contrast-to-tissue ratio and resolution [78]. Traditionally in acoustic angiography separate transducers were used for the transmitter and the receiver, however the latest approach aims at employing a single transducer for both functions. Tuning of the bias voltage and exploiting the CMUT collapse mode operation [78], [79], [80], as explained previously, are viable solutions for multi-frequency operation. Another CMUT implementation employs a reduced bottom electrode and added central mass on a thin plate [77] in order to achieve broadband response: the reduced bottom electrode increases the bandwidth by focusing the electrostatic force in the central area of the membrane, where it is most effective, and by decreasing the in-cell parasitic capacitance, while the added mass on the CMUT plate allows decoupling the spring constant and the plate mass, thus breaking the trade-off between a higher pressure narrower bandwidth device and lower pressure wider bandwidth device, and tuning the higher order vibrational mode frequencies.

Together with acoustic angiography, intravascular ultrasound (IVUS) and intracardiac echocardiography (ICE) are
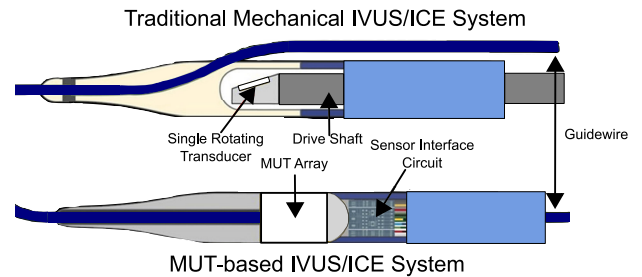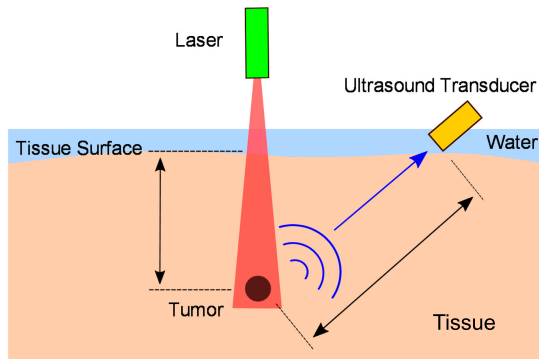

FIGURE 7. Schematic illustration of a traditional and MUT-based IVUS/ICE catheter.

also the targeted applications in the field of vascular imaging, in particular for accurate monitoring and guidance during cardiovascular interventions. Differently from acoustic angiography, IVUS and ICE are more invasive procedures as they require the insertion of a catheter, at whose tip the transducer is mounted. Traditional IVUS and ICE systems relied on a single rotating transducer [81]; however the mechanical rotation of the tip introduces rotation artefacts, and the rotation mechanism is complex to integrate with the catheter: for these reasons solid-state CMUT phased arrays [72], [82], [83], [84], [85], operating at 20-40MHz (IVUS) and 8 MHz (ICE) center frequencies, were implemented as an alternative. The traditional and MUT-based IVUS/ICE catheter, employing a solid-state phased array, are illustrated in Fig. 7.

More in detail, ICE is an ultrasound sonogram that visualizes the anatomical structure of the heart in real time: in this case the mm-scale catheter is inserted through the intracardiac vessels, and it is used to guide surgical intervention for atrial septal defect (ASD) closure. In order to solve issues of process variation in the integration of PMUT, [86] presents a 6×6 TRX pitch-matched PMUT ASIC with a standard CMOS-compatible 13.2V HV pulser, on-chip per-pixel calibration scheme, and a Dynamic Bit-Shared (DBS) ADC for portable ICE applications.

Given the small size of the catheter, the miniaturization and integration of the transducer and its electronics, together with the minimization of the number of connections, represent the most critical challenge: for this reason, CMUTs are generally preferred over PMUTs as they enable better miniaturization. The CMUT and its application-specific integrated circuit (ASIC) are connected together by means of wire-bonding [82], [83] or using a Through-Silicon-Via process [87]; parylene and silicone-like materials are used for coating the wires to ensure electrical insulation [82], [83] and flexible structures, such as the ones enabled by the so-called Flex-to-Rigid (F2R) process, are used to fit the catheter tip form factor [83], [88]. Although it is possible to delocalize some of the circuitry (e.g. the pulser) to the probe handle instead of the catheter tip by using μ-coaxial cables to connect the two [85], this is usually avoided, preferring instead to place the driver and receiver circuits close to the transducer, in order to limit the effect of parasitics

FIGURE 8. Schematic illustration of a PAI system [91].

and the bulkiness of the system [82], [83], [87], [89]. Further interconnections reduction is achieved by employing fully programmable beamformers at the transmitter side and implementing time division multiplexing at the receiver side [84].

Finally, sound impedance image and sound speed image are fused in the ultrasound computed tomography (USCT) proposed in [90] in order to obtain more information. Acoustic impedance image can provide the edges information of breast tissues, which is helpful to locate the relative position of lesion tissue. Sound speed image can provide more details of size and shape of lesion tissue, which is helpful to distinguish benign and malignant structures.

B. PHOTOACOUSTIC IMAGING

Photoacoustic imaging (PAI) is an emerging diagnostic technique which, unlike pure ultrasound imaging, does not only reflect the mechanical properties of tissues but it possesses rich optical contrast and it is capable of providing information on biofunctional or physiological parameters (e.g. oxygen saturation of hemoglobin, metabolic rate and relative concentration of water and lipid). PAI has been exploited in brain functional imaging, early cancer detection and vascular visualization; its main limitation comes from its limited imaging depth (equal to about 5 cm) due to the strong attenuation of the excitation laser in human tissues, meaning that PAI devices must be incorporated into endoscopic imaging systems to perform internal imaging diagnostics [91], [92].

In a PAI system, a short-pulsed laser, usually a laser diode in the visible to near-infrared with a collimation lens, is used to illuminate the target tissue, which absorbs optical energy and therefore experiences a rapid thermoelastic expansion: this in turn generates a pressure pulse that is sensed by an ultrasonic detector. A schematic representation of a PAI system is illustrated in Fig. 8. Multi-frequency operation is required by wideband PAI applications in order to be able to detect both high and low frequency photoacoustic content [93], thus providing optimum imaging results: here, low frequencies are used for better visualizing diffuse contrast agents distributions, while high frequencies offer fine

resolution, required for microvascular imaging and structural navigation [93].

CMUT and PMUT have been widely researched for this medical application in many recently published works. With respect to PMUTs, CMUTs are better suited to PAI applications due to their wider bandwidth and less restrictive fabrication, which allows for larger arrays, higher frequencies and dedicated geometries; however, since PMUTs rely on the established and reliable piezoelectric technology with micromachining capability, there is extensive research focused on improving the performance of PMUT that has led to promising results [94]. Literature also reports on various beamforming algorithms (delay-multiply-and-sum) to improve image quality of PMUT-based PAI [95], [96], [97]. In [98], the PZT-based PMUT array for the PAI receiving phase consists of 16×16 elements, half of which feature a resonant frequency equal to 1.2 MHz and the other half equal to 3.4 MHz. Experiments with pencil leads embedded into an agar phantom have been conducted, which clearly shows the advantages of using dual-frequency PMUT arrays to provide comprehensive images with high spatial resolution and large SNR as well. In [99] instead the array consists of 285 PZT-based PMUT elements with seven different resonant frequencies ranging from 1 MHz to 8 MHz. The developed ultrasound system can be applied specifically in endoscopic PAI for imaging multi-size targets to obtain both high resolution and large imaging depth. This system during testing has also successfully detected the pencil leads embedded in an agar phantom. Reference [100] reports on an AlN PMUT array with dual-modal endoscopic imaging (both traditional and photoacoustic imaging) in order to provide doctors with both structural and functional information for accurate diagnostics; moreover, the miniature size of PMUT shows potential for intravascular imaging within 1 mm diameter. Reference [101] shows a 65 elements PMUT array, each having 60 diaphragms of 60 μm diameter featuring a first mode resonance frequency between 6 to 8 MHz. The array was bonded to a custom-printed circuit board to enable compact integration with an optical fiber bundle and 89 % photoacoustic bandwidth was obtained. Experiments on different tissue phantoms established the feasibility of B-mode PAI for imaging targets inside optically and acoustically scattering tissues.

Studies on CMUTs for PAI applications have primarily centered on the development of 2D arrays, transparency, multi-frequency and on the challenges of photoacoustic endoscopy [102]. Concerning 2D arrays, new architectures have been introduced to facilitate addressing the various channels: for example the top orthogonal to bottom electrode (TOBE) architecture [103] requires only N bias channels and N transmit-receive channels to address each element of a N×N array.

Transparency of the transducer is required for ensuring optimal placement of the laser and illumination of the sample: in [104] transparency of up to 82% was achieved by omitting the use of silicon in the fabrication process and using instead

glass substrate and indium-tin-oxide electrodes fabricated by adhesive wafer bonding.

Multi-frequency operation is achieved in [93] by employing a CMUT array consisting of 36-μm (high frequency) and 82-μm (low frequency) cells, interlaced on a scale smaller than the smallest operating wavelength.

The challenges faced by photoacustic endoscopy are similar to the ones experienced with IVUS and ICE as the encapsulation of the transducer inside a catheter is required. In addition to phased arrays [102], [105], ring arrays are also employed [106]: although ring arrays are generally more complicated to design and fabricate, the circular view that they provide gives a wider field of view and reduces the occurrence of reconstruction artifacts, while making use of the empty spaces around the probe thus optimizing the available space [102].

In order to improve the image quality, multi-perspective PAI can be employed [107], [108]: an approach employing a pair of linear arrays was proposed in [107], while a system based on multiple spatially separated CMUTs with shared communication channels where the imaging process is achieved by multiplexing the signals in time was presented in [108].

C. ULTRASOUND-BASED THERAPY

The use of ultrasound is not limited to diagnostic applications, but it can also be therapeutical: focused ultrasound can be employed for neurostimulation [109], [110], [111], [112], [113], [114], [115], [116], [117], [118], [119], [120], [121], [122] as well as for thermal ablation (e.g. for tumor treatment), when high-intensity focused ultrasound (HIFU) is used [123], [124], [125], [126], [127], [128]. Ultrasound neurostimulation is used non-invasively [110] for stimulating the brain, peripheral nervous system [117], [118], [119], [129], and retina [130]. Administering ultrasound via implantable devices is also being investigated as a means to increase the spatial selectivity in peripheral nerve neuromodulation [114], [115], [131]. On the other hand, HIFU can be administered externally or with minimal invasion, such as through body orifices, endoscopic incisions, or intravascularly via catheters [125]. This approach is similar to IVUS and ICE, presenting similar challenges in miniaturization. Furthermore, implantable ultrasound devices can also be used to wirelessly monitor temperature increase during HIFU or LIFU [129], [132].

Therapeutic focused ultrasound devices consist of bowl-shaped single-element transducers for fixed focus operation or transducer arrays, which allow adapting the ultrasound beam pattern according to the geometry and location of the target regions, by means of dedicated electronic driving. Single-element transducers are typically bulk PZT-based devices, while arrays can be implemented with either bulk-transducers [121], [133] or MUT technology [112]. Bulk-transducer integration with silicon substrates, such as in the case of CMOS technology, requires complex fabrication steps

to mitigate unwanted acoustic absorption at the substrate level [134]. On the other hand, the MUT fabrication process benefits from easier integration with CMOS technology, which allows for higher miniaturization capabilities and design flexibility. Furthermore, both neurostimulation and HIFU applications typically require image guidance, which can be provided through MRI [124], [125] or ultrasound imaging [113], [123], [128]. MUTs are composed of MRI-compatible materials [126], which is an added benefit in comparison with bulk-transducers, typically implemented with PZT.

Several works exploring the above-mentioned properties have been described in the literature. In [124] a 32 × 32 elements 2D CMUT array, flip-chip bonded to the ASIC on a flexible PCB, was proposed: the system, designed for HIFU catheter applications exploited the same transducer both for HIFU and ultrasound imaging. A planar dual mode CMUT probe consisting of a 3 MHz, 64-element annular array for therapy and 7 MHz, 256-element linear array for imaging were investigated through simulation and experimentally in [123], while the design and creation of a fully integrated HIFU drive system on a chip, intended for a 6 Fr catheter probe, was showcased in [125], employing an 8-element CMUT ring array of 2 mm diameter as the ultrasound source. In [126] a 32 × 32 elements 2D CMUT array for HIFU applications was presented. To reduce the system complexity for addressing the 1024 transducer elements, the CMUT array elements were grouped into eight HIFU channels based on the phase delay from the CMUT element to the targeted focal point. Ex vivo tissue experiments successfully demonstrated its capability to make lesions in both bovine muscle and liver tissue.

In [127] the electroacoustic performance of CMUTs designed for interstitial high-intensity contact (HICU) ultrasound (US) applications was evaluated and the feasibility of generating US-induced heating and thermal destruction of biological tissues was studied. One-dimensional CMUT linear arrays as well as a prism-shaped 2-D array composed of multiple 1-D linear arrays mounted on a cylindrical catheter were fabricated. Irreversible thermal damage was produced in turkey breast tissue samples. The CMUT prototypes tested herein were capable of generating significant US-induced thermal heating in tissue-mimicking phantoms and in in-vitro tissue samples without the need for an external cooling system. The bias voltage plays a significant role in the optimization of the CMUT intensity output, as well as the collapse-snapback operative regime.

A front-end integrated circuit (IC) for an ultrasound neurostimulation system, interfaced with a 16×16 2D CMUT array to establish an ultrasound field pattern (USFP) using quantized phases and amplitudes, was demonstrated in [110], while a 2D ultrasonic transmit phased array based on a 32×32 CMUT array flip-chip bonded to a pitch-matched pulser ASIC for ultrasonic neuromodulation was proposed in [112]. Finally, in [111] a wearable ultrasonic neural stimulator for chronic implantation in rats is shown where a

16-element 1D linear CMUT array bonded to the electronics of the neurostimulator was implanted on the rat's brain. The electronics includes the ASIC, power management unit (PMU), a wireless-module and battery which were contained in a backpack of the rat to distribute the weight of the whole wearable device.

In [114] and [115] a flexible CMUT array has been curved to 1 mm radius to wrap around the vagus nerve and deliver spatially specific stimulation. The CMUT array operated at 15 MHz and had a focal spot of 110 μm and 550 μm, which is only 2.1% of the cross section of the nerve [114]. Peak negative acoustic pressures of 1.7 MPa were demonstrated while beam-steering moved the focal spot to arbitrary locations within the focal plane of the transducer array [115]. An analogous work with PZTs showed higher transmit sensitivity ($S_{tx} = 160$ kPa/V) at the expense of ease of integration [131].

MUTs have also been integrated with microelectrodes and proposed as bimodal neuroscientific investigation tools. In [116] electrodes were non-monolithically fabricated on top of PMUT arrays to elucidate neural response to electrical and ultrasonic stimuli.

D. IMPLANTABLE DEVICES

Ultrasound transducers are of interest for the biomedical field not only for their direct application in diagnostics and therapy, but also for enabling powering and communication to the implantable devices. Indeed, compared to the radio-frequency (RF) technology, ultrasound offers numerous benefits: the maximum allowed power level in tissue for diagnostic ultrasound is roughly 70 times higher compared to RF energy limits, the attenuation of ultrasonic signals in tissue is far less than RF, and despite its shorter wavelength with respect to RF, ultrasound can be precisely focused, delivering energy to large penetration depths (> 5 cm), while requiring smaller sized receivers [135].

Commonly, PZT-based transducers are used to convert acoustic energy into electrical energy. Unfortunately, these lead containing devices require hermetic encapsulation for them to be implanted inside the body, and this severely degrades their energy-efficiency [136]. Other lead-free piezo-electric materials that are biocompatible, such as polyvinyli-dene fluoride (PVDF) and barium titanate ($BaTiO_3$), have been investigated, however their piezoelectric constants are significantly lower compared to the conventional PZT. Additionally, also AlN-based PMUTs and CMUTs have been studied, although AlN PMUTs feature good piezoelectric properties, their operation frequency is larger, thus determining a higher ultrasound attenuation along its travelling path; CMUTs, on the other hand, support traditional ultrasound frequencies, in the range of a few-to-tens of MHz while also allowing seamless integration in CMOS processes [136]. The main disadvantage of CMUTs is the required higher bias voltage, which can reach more than 100 V and is clearly not suitable for wearable or implantable applications where

a low-voltage source like a battery needs to be used instead: the need for high external bias voltages, however, can be eliminated by creating a built-in bias voltage through charge trapping Al_2O_3 layer inside the CMUT [136].

In [137] an investigation is presented on a micromachined ultrasonic power-generating receiver that is capable of providing adequate power for implantable medical devices. The main issue addressed in this work is that the PMUT must be small enough to be used as an implantable and also it must be operational at low frequencies to reduce attenuation in tissues. Simulation shown in the paper reports that the thickness of the piezoelectric layer must be of 6 to 100 microns, and since conventional deposition techniques cannot produce such thicker films, the paper reports on using a bulk PZT layer and polishing it down to the desired thickness corresponding to the required frequency, enabling millimeter scale bending diaphragm as well.

In [138], a zero-power ultrasonic wakeup receiver for intra-body communication with implantable medical devices is exhibited. This was demonstrated in a tissue phantom for use in Internet of Medical Things (IoMT) applications. In this promising application, the devices are designed to be installed by the healthcare providers into the patients, who in turn, although they cannot access them directly, are able to collect data from these smart sensors (e.g., into the smartphone) in order to share useful information to hospitals and clinics. PMUTs are good candidates for this application thanks to their biocompatibility, small form-factors and their operation at low bias voltages. For this reason, in order to reduce the power consumption, this work proposes to keep off the main power hungry communication module and to activate it upon the reception of an incoming ultrasonic signal. The system is implemented using a 10×10 AlN PMUT array, a zero-power 500 nm gap MEMS plasmonic switch, a low-leakage CMOS load switch and a specific ad hoc sensing circuit.

An example of CMUT-based implanted device is the post-operative monitoring of abdominal aortic aneurysm repair: the tiny ultrasonically powered device integrated into the Endo-Vascular Aneurysm Repair (EVAR) stent-graft, and delivered trans-cutaneously, illustrated in [135], can provide on demand diagnostic information about the presence of endoleaks, based on measurements of the aneurysm sack dimensions and of the stent-graft inside the vessel lumen, while supporting high data rate thanks to the ultrasonic biphasic communication concept. The functionality of the wireless ultrasonic power recovery scheme to power the device was demonstrated in oil using a single-element CMUT. Ultrasound power can be delivered to an implantable device using either a single element transducer or a phased array transducer: single element transducers allow powering multiple implants, however a significant amount of power will be lost at the locations in between the implants, also increasing the risk of possible damage to the surrounding tissue; phased array transducers, instead, focus the output power on the target implant, thus maximizing the power transfer efficiency. For these reasons communication and

power transfer to a single implant at a time is generally preferred. In phased arrays, however, the sensitivity to beam misalignments can cause sharp decrease in the amount of transferred power and quality of communication. In a real case scenario, the position of the receiver implant is not known a priori and can change over time due to body motions. Hence a traditional ultrasound scan and the employment of tracking algorithms to locate the implant are usually required. Implant localization can be realized in an active or passive manner: active tracking requires the active driving of the ultrasound transducer on the implant and offers a greater penetration depth, while passive tracking uses an ultrasound wave sent by an external transmitter that is backscattered by the implant transducer element and requires significantly lower power consumption. The use of a passive tracking telemetry protocol, relying on the phase difference of the ultrasound signal backscattered by the implant and received by each element of a linear phased array, is investigated in [139], in order to precisely focus the ultrasound beam on the implant and create a tight ultrasound link robust against small movements.

E. OTHER MEDICAL APPLICATIONS

Wearable devices and continuous monitoring nowadays are leading the way for early detection of many conditions, such as heart and lung diseases, but also for muscle disorder diagnostics and rehabilitation training. PMUTs are ideal for real-time monitoring due to their characteristics such as miniaturized form-factor, acoustic connectivity, cost-effective production, energy efficiency, and the absence of the requirement for a high bias voltage (unlike CMUTs, where high bias voltage is needed to drive them). In this field, we highlight [140], a work on a dual electrode bimorph AlN PMUT to be used for muscle monitoring. In this paper, both A- and B-mode scans are reported to have been implemented in order to successfully detect three different kinds of phantoms by the pulse-echo measurements; [141] shows an AlN based PMUT for continuous monitoring of the mechano-acoustic cardiopulmonary signals, specifically the sensing of the heart rate, heart sound, respiratory rate and lung sound. The sensing cells of the reported PMUTs are designed and arranged as honeycomb architecture in order to achieve high fill-factor, but also to enhance the acoustic sensitivity. In [142], a pulsed-wave doppler ultrasound blood flowmeter is developed using AlN PMUTs for non-invasive and wearable blood flow measurements. In this work, a compensation process containing linear fitting, slopping, and intercept calibration has been utilized in order to improve the accuracy. Reference [143] illustrates a prototype of a high-sensitivity and wearable bowel sound monitor based on an AlN PMUT array. The sensing module is composed of four PMUTs connected in parallel and a signal conditioning circuit, achieving high sensitivity, high noise resolution and small non-linearity.

Another interesting PMUT utilization in the medical field is fluid monitoring and, more specifically, the integration with microfluidic technologies: [144] shows a study on the potential development of a real-time fluid density monitoring system for hemoglobin concentration using a dual electrode, self-sensing PZT PMUT integrated with a microfluidic channel. In particular, the sensitivity of the sensor (26.3 Hz/(kg/m^3)) is good enough to reliably detect even 1% change in the hemoglobin content of the human blood.

A novel area of application for MUTs devices is inhalation therapy, where MUTs are employed for implementing vibrating mesh nebulizers. These devices are typically made with a metal-based circular membrane operated at the second harmonic and moved by a PZT actuator [145]; however the pronounced self-heating effect of piezoelectric materials and the need for stability over time and reusable devices considering the technology cost have pushed the research towards CMUTs. An example of CMUT based nebulizer is proposed in [146]: the nebulizer silicon membrane is obtained from a bulk silicon substrate that is locally etched on the backside in order to obtain a membrane that is clamped, on its periphery, to the bulk substrate; the membrane is actuated by a CMUT array placed at the center of the membrane and fabricated directly on the substrate. The geometry of the CMUT array follows the mesh, i.e. circular, with dimensions smaller to leave place for holes for drug atomization and aerosol production. The CMUTs are engineered such that their distinct resonance frequency lies in the MHz range, but it is not aligned with the typical operating frequency (around 100 kHz) of the mesh nebulizer. In this context, the CMUTs vibrates similarly to a microphone, functioning in a purely elastic mode.

Additional medical employment for MUTs include the implementation of a laparoscope [147] and vibration-controlled transient elastography for the assessment of liver fibrosis and steatosis [148]. Due to the limited space in the laparoscope, analogously to endoscopic ultrasound applications, CMUT is preferred. Concerning the elastography applications, both PZT and CMUT technology can be used: CMUTs, due to their broader frequency band, can enable real-time tuning of the working frequency in order to avoid the signal degradation arising from tissue attenuation, often due to the patient morphology (e.g. the presence of subcutaneous fat) [148].

V. CONCLUSION

In this paper the PMUTs and CMUTs as next generation transducers employed for biomedical applications were investigated, describing in detail their respective advantages and limitations. Their physical working principle has been reported and extensively explained as well as the materials and methods employed in their fabrication process. Their most prominent medical employments nowadays are reported and many recently published works are illustrated in order to suggest where future innovations will be headed for healthcare applications. It has been discovered that CMUTs currently provide broader possibilities in this area, attributed

to their numerous advantages. These include a wider bandwidth and improved resolution, a more straightforward fabrication process, ease of integration with ASICs, and their capability to operate effectively at high frequencies. PMUTs, on the other hand, show many promising features that may help making them more relevant in the future, although today they are not a dominating alternative to CMUTs in bioelectronics. Their main benefits are, in contrast to CMUTs, the lack of a high bias voltage (so that devices can be used as wearable sensors which are driven by a low-voltage source like battery), and lower sensitivity to parasitics. Their bandwidth and resolution limitation on the other hand could be improved with advancements in the fabrication and design process in order to push even further in the development of next generation ultrasound devices.

REFERENCES

[1] I. Donald, J. Macvicar, and T. G. Brown, "Investigation of abdominal masses by pulsed ultrasound," *Lancet*, vol. 271, no. 7032, pp. 1188–1195, Jun. 1958. [Online]. Available: https://www.sciencedirect.com/science/article/pii/S0140673658919056

[2] I. Zamora, E. Ledesma, A. Uranga, and N. Barniol, "Miniaturized 0.13-μm CMOS front-end analog for AlN PMUT arrays," *Sensors*, vol. 20, no. 4, p. 1205, Feb. 2020.

[3] Y. Birjis, S. Swaminathan, H. Nazemi, G. C. A. Raj, P. Munirathinam, A. Abu-Libdeh, and A. Emadi, "Piezoelectric micromachined ultrasonic transducers (PMUTs): Performance metrics, advancements, and applications," *Sensors*, vol. 22, no. 23, p. 9151, Nov. 2022.

[4] Q. Zhou, K. H. Lam, H. Zheng, W. Qiu, and K. K. Shung, "Piezoelectric single crystal ultrasonic transducers for biomedical applications," *Prog. Mater. Sci.*, vol. 66, pp. 87–111, Oct. 2014.

[5] J. Joseph, B. Ma, and B. T. Khuri-Yakub, "Applications of capacitive micromachined ultrasonic transducers: A comprehensive review," *IEEE Trans. Ultrason., Ferroelectr., Freq. Control*, vol. 69, no. 2, pp. 456–467, Feb. 2022.

[6] K. Roy, H. Gupta, V. Shastri, A. Dangi, A. Jeyaseelan, S. Dutta, and R. Pratap, "Fluid density sensing using piezoelectric micromachined ultrasound transducers," *IEEE Sensors J.*, vol. 20, no. 13, pp. 6802–6809, Jul. 2020.

[7] K. Roy, H. Gupta, V. Shastri, A. Dangi, and R. Pratap, "Fluid density sensing using PMUTs," in *Proc. IEEE Sensors*, Oct. 2018, pp. 1–4.

[8] K. Roy, K. Kalyan, A. Ashok, V. Shastri, and R. Pratap, "A pmut integrated microfluidic system for volumetric flow rate sensing," in *Proc. 21st Int. Conf. Solid-State Sensors, Actuators Microsyst.*, Jun. 2021, pp. 172–175.

[9] C. Sun, Q. Shi, M. Yazici, C. Lee, and Y. Liu, "Development of a highly sensitive humidity sensor based on a piezoelectric micromachined ultrasonic transducer array functionalized with graphene oxide thin film," *Sensors*, vol. 18, no. 12, p. 4352, Dec. 2018.

[10] S. Sun, J. Wang, M. Zhang, Y. Yuan, Y. Ning, D. Ma, P. Niu, Y. Gong, X. Yang, and W. Pang, "Eye-tracking monitoring based on PMUT arrays," *J. Microelectromech. Syst.*, vol. 31, no. 1, pp. 45–53, Feb. 2022.

[11] C. Y. Cheng, A. Dangi, L. Ren, S. Tiwari, R. R. Benoit, Y. Qiu, H. S. Lay, S. Agrawal, R. Pratap, S.-R. Kothapalli, T. E. Mallouk, S. Cochran, and S. Trolier-Mckinstry, "Thin film PZT-based PMUT arrays for deterministic particle manipulation," *IEEE Trans. Ultrason., Ferroelectr., Freq. Control*, vol. 66, no. 10, pp. 1606–1615, Oct. 2019.

[12] H. Nazemi, J. Antony Balasingam, S. Swaminathan, K. Ambrose, M. U. Nathani, T. Ahmadi, Y. Babu Lopez, and A. Emadi, "Mass sensors based on capacitive and piezoelectric micromachined ultrasonic transducers—CMUT and PMUT," *Sensors*, vol. 20, no. 7, p. 2010, Apr. 2020.

[13] D. A. Hutchins, D. R. Billson, R. J. Bradley, and K. S. Ho, "Structural health monitoring using polymer-based capacitive micromachined ultrasonic transducers (CMUTs)," *Ultrasonics*, vol. 51, no. 8, pp. 870–877, Dec. 2011.

[14] L. Capineri and A. Bulletti, "Ultrasonic guided-waves sensors and integrated structural health monitoring systems for impact detection and localization: A review," *Sensors*, vol. 21, no. 9, p. 2929, Apr. 2021.

[15] Y. He, H. Wan, X. Jiang, and C. Peng, "Piezoelectric micromachined ultrasound transducer technology: Recent advances and applications," *Biosensors*, vol. 13, no. 1, p. 55, Dec. 2022.

[16] K. Smyth and S. Kim, "Experiment and simulation validated analytical equivalent circuit model for piezoelectric micromachined ultrasonic transducers," *IEEE Trans. Ultrason., Ferroelectr., Freq. Control*, vol. 62, no. 4, pp. 744–765, Apr. 2015.

[17] F. Pop, B. Herrera, C. Cassella, and M. Rinaldi, "Modeling and optimization of directly modulated piezoelectric micromachined ultrasonic transducers," *Sensors*, vol. 21, no. 1, p. 157, Dec. 2020.

[18] J. E. Aldrich, "Basic physics of ultrasound imaging," *Crit. Care Med.*, vol. 35, pp. S131–S137, May 2007.

[19] M. Trindade and A. Benjeddou, "Effective electromechanical coupling coefficients of piezoelectric adaptive structures: Critical evaluation and optimization," *Mech. Adv. Mater. Struct.*, vol. 16, no. 3, pp. 210–223, Apr. 2009.

[20] K. Roy, J. E.-Y. Lee, and C. Lee, "Thin-film PMUTs: A review of over 40 years of research," *Microsyst. Nanoeng.*, vol. 9, no. 1, pp. 1–15, Jul. 2023.

[21] Y. Qiu, J. Gigliotti, M. Wallace, F. Griggio, C. Demore, S. Cochran, and S. Trolier-McKinstry, "Piezoelectric micromachined ultrasound transducer (PMUT) arrays for integrated sensing, actuation and imaging," *Sensors*, vol. 15, no. 4, pp. 8020–8041, Apr. 2015.

[22] L. Jia, L. Shi, C. Liu, C. Sun, and G. Wu, "Enhancement of transmitting sensitivity of piezoelectric micromachined ultrasonic transducers by electrode design," *IEEE Trans. Ultrason., Ferroelectr., Freq. Control*, vol. 68, no. 11, pp. 3371–3377, Nov. 2021.

[23] E. Ledesma, I. Zamora, A. Uranga, and N. Barniol, "Tent-plate AlN PMUT with a piston-like shape under liquid operation," *IEEE Sensors J.*, vol. 20, no. 19, pp. 11128–11137, Oct. 2020.

[24] P. N. Thao, S. Yoshida, and S. Tanaka, "Development of mechanically-robust piezoelectric micromachined ultrasonic transducer (pMUT) with island-shaped PZT monocrystalline thin film," in *Proc. 20th Int. Conf. Solid-State Sensors, Actuat. Microsystems Eurosensors*, Jun. 2019, pp. 833–836.

[25] Q. Yu, G. Fan, W. Ren, Q. Fan, J. Ti, J. Li, and C. Wang, "PZT-film-based piezoelectric micromachined ultrasonic transducer with I-shaped composite diaphragm," *Micromachines*, vol. 13, no. 10, p. 1597, Sep. 2022.

[26] S. Akhbari, F. Sammoura, C. Yang, M. Mahmoud, N. Aqab, and L. Lin, "Bimorph pMUT with dual electrodes," in *Proc. 28th IEEE Int. Conf. Micro Electro Mech. Syst. (MEMS)*, Jan. 2015, pp. 928–931.

[27] S. Wu, W. Li, D. Jiao, H. Yang, T. Wu, and X. Li, "An aluminum-nitride PMUT with pre-concaved membrane for large deformation and high quality-factor performance," in *Proc. 21st Int. Conf. Solid-State Sensors, Actuators Microsystems*, Jun. 2021, pp. 46–49.

[28] R. Manwar and S. Chowdhury, "Experimental analysis of bisbenzo-cyclobutene bonded capacitive micromachined ultrasonic transducers," *Sensors*, vol. 16, no. 7, p. 959, Jun. 2016.

[29] H. Wang, X. Huang, L. Yu, Q. Ding, H. Zhang, C. He, and W. Zhang, "Hybrid cell structure for wideband CMUT: Design method and characteristic analysis," *Micromachines*, vol. 12, no. 10, p. 1180, Sep. 2021.

[30] A. Stuart Savoia, B. Mauti, L. Fanni, A. Bagolini, E. Boni, A. Ramalli, F. Guanziroli, S. Passi, M. Sautto, G. Matrone, R. Bardelli, P. Bellutti, F. Quaglia, G. Caliano, A. Mazzanti, and P. Tortoli, "A 256-element spiral CMUT array with integrated analog front end and transmit beamforming circuits," in *Proc. IEEE Int. Ultrason. Symp. (IUS)*, Oct. 2018, pp. 206–212.

[31] K. Brenner, A. Ergun, K. Firouzi, M. Rasmussen, Q. Stedman, and B. Khuri-Yakub, "Advances in capacitive micromachined ultrasonic transducers," *Micromachines*, vol. 10, no. 2, p. 152, Feb. 2019.

[32] J. Wang, X. Liu, Y. Yu, Y. Li, C. Cheng, S. Zhang, P. Mak, M. Vai, and S. Pun, "A review on analytical modeling for collapse mode capacitive micromachined ultrasonic transducer of the collapse voltage and the static membrane deflections," *Micromachines*, vol. 12, no. 6, p. 714, Jun. 2021.

[33] J. Ling, Y.-Q. Chen, Y. Chen, D.-Y. Wang, Y.-F. Zhao, Y. Pang, Y. Yang, and T.-L. Ren, "Design and characterization of high-density ultrasonic transducer array," *IEEE Sensors J.*, vol. 18, no. 6, pp. 2285–2290, Mar. 2018.

[34] D. Bokov, A. Turki Jalil, S. Chupradit, W. Suksatan, M. Javed Ansari, I. H. Shewael, G. H. Valiev, and E. Kianfar, "Nanomaterial by sol-gel method: Synthesis and application," *Adv. Mater. Sci. Eng.*, vol. 2021, pp. 1–21, Dec. 2021.

[35] F. Griggio, C. E. M. Demore, H. Kim, J. Gigliotti, Y. Qiu, T. N. Jackson, K. Choi, R. L. Tutwiler, S. Cochran, and S. Trolier-McKinstry, "Micromachined diaphragm transducers for miniaturised ultrasound arrays," in *Proc. IEEE Int. Ultrason. Symp.*, Oct. 2012, pp. 1–4.

[36] A. Robichaud, D. Deslandes, P.-V. Cicek, and F. Nabki, "A novel topology for process variation-tolerant piezoelectric micromachined ultrasonic transducers," *J. Microelectromech. Syst.*, vol. 27, no. 6, pp. 1204–1212, Dec. 2018, doi: 10.1109/JMEMS.2018.2876384.

[37] B. Yu, C. Yu, L. Zhang, Z. Wang, X. Xu, A. He, X. Wang, P. Niu, and W. Pang, "Cost-effective strategy for developing small sized high frequency PMUTs toward phased array imaging applications," *J. Microelectromech. Syst.*, vol. 32, no. 2, pp. 164–172, Apr. 2023.

[38] D. E. Dausch, J. B. Castellucci, D. R. Chou, and O. T. von Ramm, "Theory and operation of 2-D array piezoelectric micromachined ultrasound transducers," *IEEE Trans. Ultrason., Ferroelectr., Freq. Control*, vol. 55, no. 11, pp. 2484–2492, Nov. 2008.

[39] H. Wang, Y. Yu, Z. Chen, H. Yang, H. Jiang, and H. Xie, "Design and fabrication of a piezoelectric micromachined ultrasonic transducer array based on ceramic PZT," in *Proc. IEEE Sensors*, Oct. 2018, pp. 1–4.

[40] E. Ledesma, I. Zamora, A. Uranga, and N. Barniol, "Multielement ring array based on minute size PMUTs for high acoustic pressure and tunable focus depth," *Sensors*, vol. 21, no. 14, p. 4786, Jul. 2021.

[41] G.-L. Luo and D. A. Horsley, "Piezoelectric micromachined ultrasonic transducers with corrugated diaphragms using surface micromachining," in *Proc. 20th Int. Conf. Solid-State Sensors, Actuators Microsyst. Eurosensors*, Jun. 2019, pp. 841–844.

[42] Q. Wang, Y. Lu, S. Mishin, Y. Oshmyansky, and D. A. Horsley, "Design, fabrication, and characterization of scandium aluminum nitride-based piezoelectric micromachined ultrasonic transducers," *J. Microelectromech. Syst.*, vol. 26, no. 5, pp. 1132–1139, Oct. 2017, doi: 10.1109/JMEMS.2017.2712101.

[43] Y. Kusano, I. Ishii, T. Kamiya, A. Teshigahara, G.-L. Luo, and D. A. Horsley, "High-SPL air-coupled piezoelectric micromachined ultrasonic transducers based on 36% ScAlN thin-film," *IEEE Trans. Ultrason., Ferroelectr., Freq. Control*, vol. 66, no. 9, pp. 1488–1496, Sep. 2019.

[44] K. Bespalova, E. Österlund, G. Ross, M. Paulasto-Kröckel, A. T. Sebastian, C. B. Karuthedath, S. Mertin, and T. Pensala, "Characterization of AlScN-based multilayer systems for piezoelectric micromachined ultrasound transducer (pMUT) fabrication," *J. Microelectromech. Syst.*, vol. 30, no. 2, pp. 290–298, Apr. 2021.

[45] R. Lu, M. Breen, A. E. Hassanien, Y. Yang, and S. Gong, "A piezoelectric micromachined ultrasonic transducer using thin-film lithium niobate," *J. Microelectromech. Syst.*, vol. 29, no. 6, pp. 1412–1414, Dec. 2020.

[46] K. Suzuki, Y. Nakayama, I. Kanagawa, Y. Matsushita, T. Mizuno, Y. Mita, and T. Yoshimura, "Monolithic integration of P(VDF-TrFE) thin film on CMOS for wide-band ultrasonic transducer arrays," in *Proc. IEEE Int. Ultrason. Symp. (IUS)*, Oct. 2019, pp. 807–810.

[47] J. Li, W. Ren, G. Fan, and C. Wang, "Design and fabrication of piezoelectric micromachined ultrasound transducer (pMUT) with partially-etched ZnO film," *Sensors*, vol. 17, no. 6, p. 1381, Jun. 2017.

[48] S. Sun, M. Zhang, C. Gao, B. Liu, and W. Pang, "Flexible piezoelectric micromachined ultrasonic transducers towards new applications," in *Proc. IEEE Int. Ultrason. Symp. (IUS)*, Oct. 2018, pp. 1–4.

[49] S. Sadeghpour, B. Lips, M. Kraft, and R. Puers, "Bendable piezoelectric micromachined ultrasound transducer (PMUT) arrays based on silicon-on-insulator (SOI) technology," *J. Microelectromech. Syst.*, vol. 29, no. 3, pp. 378–386, Jun. 2020.

[50] K. Suzuki, Y. Nakayama, N. Shimizu, and T. Mizuno, "Study on wideband piezoelectric micro-machined ultrasound transducers (pMUT) by combined resonance frequencies and controlling poling directions," in *Proc. IEEE Int. Ultrason. Symp. (IUS)*, Oct. 2018, pp. 1–3.

[51] L. Wu, M. Moridi, G. Wang, and Q. Zhou, "Microfabrication and characterization of dual-frequency piezoelectric micromachined ultrasonic transducers," in *Proc. IEEE Int. Symp. Appl. Ferroelectr. (ISAF)*, May 2021, pp. 1–4.

[52] H. Gao, P. Gijsenbergh, A. Halbach, C. P. Serrahima, G. B. Torri, Y. Jeong, M. Billen, D. Cheyns, R. Haouari, X. Rottenberg, and V. Rochus, "Design of polymer-based PMUT array for multi-frequency ultrasound imaging," in *Proc. IEEE Int. Ultrason. Symp. (IUS)*, Oct. 2019, pp. 1092–1095.

[53] X. Huang, H. Wang, and L. Yu, "Investigation on design theory and performance analysis of vacuum capacitive micromachined ultrasonic transducer," *Micromachines*, vol. 12, no. 9, p. 1127, Sep. 2021.

[54] F. Yildiz, T. Matsunaga, and Y. Haga, "Fabrication and packaging of CMUT using low temperature co-fired ceramic," *Micromachines*, vol. 9, no. 11, p. 553, Oct. 2018.

[55] C. He, B. Zhang, C. Xue, W. Zhang, and S. Zhang, "Wafer-bonding fabricated CMUT device with parylene coating," *Micromachines*, vol. 12, no. 5, p. 516, May 2021.

[56] K. K. Park, H. Lee, M. Kupnik, and B. T. Khuri-Yakub, "Fabrication of capacitive micromachined ultrasonic transducers via local oxidation and direct wafer bonding," *J. Microelectromech. Syst.*, vol. 20, no. 1, pp. 95–103, Feb. 2011.

[57] X. Wang, Y. Yu, and J. Ning, "Fabrication and characterization of capacitive micromachined ultrasonic transducers with low-temperature wafer direct bonding," *Micromachines*, vol. 7, no. 12, p. 226, Dec. 2016.

[58] I. Lucarini, L. Maiolo, and A. S. Savoia, "Fabrication and characterization of capacitive micromachined ultrasonic transducers integrated on ultra-thin and flexible substrates," in *Proc. IEEE Int. Ultrason. Symp. (IUS)*, Oct. 2019, pp. 778–780.

[59] I. Lucarini, L. Maiolo, F. Maita, and A. Savoia, "Demonstration of PolyimideBased flexible CMUT operation on curved substrates," in *Proc. IEEE Int. Ultrason. Symp. (IUS)*, Sep. 2021, pp. 1–3.

[60] A. Omidvar, C. D. Gerardo, R. Rohling, E. Cretu, and A. J. Hodgson, "Flexible polymer-based capacitive micromachined ultrasound transducers (polyCMUTs): Fabrication and characterization," in *Proc. IEEE Int. Ultrason. Symp. (IUS)*, Sep. 2021, pp. 1–3.

[61] M. Maadi, C. Ceroici, and R. J. Zemp, "Dual-frequency CMUT arrays for multiband ultrasound imaging applications," *IEEE Trans. Ultrason., Ferroelectr., Freq. Control*, vol. 68, no. 7, pp. 2532–2542, Jul. 2021.

[62] M. D. C. Eames, T. J. Reck, and J. A. Hossack, "Selectable frequency CMUT with membrane stand-off structures," in *Proc. IEEE Int. Ultrason. Symp.*, Sep. 2009, pp. 2814–2817.

[63] M. Pekař, W. U. Dittmer, N. Mihajlović, G. van Soest, and N. de Jong, "Frequency tuning of collapse-mode capacitive micromachined ultrasonic transducer," *Ultrasonics*, vol. 74, pp. 144–152, Feb. 2017.

[64] T. L. Szabo, *Diagnostic Ultrasound Imaging: Inside Out*. Amsterdam, The Netherlands: Elsevier, 2004.

[65] Z. Wang, C. He, W. Zhang, Y. Li, P. Gao, Y. Meng, G. Zhang, Y. Yang, R. Wang, J. Cui, H. Wang, B. Zhang, Y. Ren, G. Zhen, X. Jiao, and S. Zhang, "Fabrication of 2-D capacitive micromachined ultrasonic transducer (CMUT) array through silicon wafer bonding," *Micromachines*, vol. 13, no. 1, p. 99, Jan. 2022.

[66] T. A. Emadi and D. A. Buchanan, "A novel 6 × 6 element MEMS capacitive ultrasonic transducer with multiple moving membranes for high performance imaging applications," *Sens. Actuators A, Phys.*, vol. 222, pp. 309–313, Feb. 2015.

[67] R. O. Guldiken, J. Zahorian, F. Y. Yamaner, and F. L. Degertekin, "Dual-electrode CMUT with non-uniform membranes for high electromechanical coupling coefficient and high bandwidth operation," *IEEE Trans. Ultrason., Ferroelectr., Freq. Control*, vol. 56, no. 6, pp. 1270–1276, Jun. 2009.

[68] T.-C. Cheng, Y.-T. Liao, and T.-H. Tsai, "High-sensitivity CMUT with interlayer metal architecture for medical ultrasonic systems," in *Proc. 18th Int. Conf. Solid-State Sensors, Actuators Microsyst.*, Jun. 2015, pp. 1211–1214.

[69] T.-C. Cheng and T.-H. Tsai, "CMOS ultrasonic receiver with on-chip analog-to-digital front end for high-resolution ultrasound imaging systems," *IEEE Sensors J.*, vol. 16, no. 20, pp. 7454–7463, Oct. 2016.

[70] R. S. Grass, A. S. Havreland, M. Engholm, J. A. Jensen, and E. V. Thomsen, "188+188 row–column addressed CMUT transducer for super resolution imaging," in *Proc. IEEE Int. Ultrason. Symp. (IUS)*, Oct. 2019, pp. 746–749.

[71] O. J. Adelegan, T. I. Minhaj, Z. A. Coutant, F. Y. Yamaner, and Ö. Oralkan, "Forming an annular array from 2D capacitive micromachined ultrasonic transducer (CMUT) array elements by using a metal redistribution layer," in *Proc. IEEE Int. Ultrason. Symp. (IUS)*, Sep. 2020, pp. 1–3.

[72] S. Lee and J. Ikeda, "A study of an annular array CMUT device for the making of forward looking IVUS," in *Proc. IEEE Int. Ultrason. Symp. (IUS)*, Sep. 2021, pp. 1–4.

[73] E. Shin, H. G. Yeo, A. Yeon, C. Jin, W. Park, S.-C. Lee, and H. Choi, "Development of a high-density piezoelectric micromachined ultrasonic transducer array based on patterned aluminum nitride thin film," *Micromachines*, vol. 11, no. 6, p. 623, Jun. 2020.

[74] A. S. Savoia, M. Casavola, E. Boni, M. Ferrera, C. Prelini, P. Tortoli, D. Giusti, and F. Quaglia, "Design, fabrication, characterization, and system integration of a 1-D PMUT array for medical ultrasound imaging," in *Proc. IEEE Int. Ultrason. Symp. (IUS)*, Sep. 2021, pp. 1–3.

[75] S. Sadeghpour, S. V. Joshi, C. Wang, and M. Kraft, "Novel phased array piezoelectric micromachined ultrasound transducers (pMUTs) for medical imaging," *IEEE Open J. Ultrason., Ferroelectr., Freq. Control*, vol. 2, pp. 194–202, 2022.

[76] C. Liu, B. Zhang, C. Xue, W. Zhang, G. Zhang, and Y. Cheng, "Multi-perspective ultrasound imaging technology of the breast with cylindrical motion of linear arrays," *Appl. Sci.*, vol. 9, no. 3, p. 419, Jan. 2019.

[77] J. L. Sanders, A. Ö. Biliroglu, I. G. Newsome, O. J. Adelegan, F. Y. Yamaner, P. A. Dayton, and Ö. Oralkan, "A handheld imaging probe for acoustic angiography with an ultrawideband capacitive micromachined ultrasonic transducer (CMUT) array," *IEEE Trans. Ultrason., Ferroelectr., Freq. Control*, vol. 69, no. 7, pp. 2318–2330, Jul. 2022.

[78] M. M. Mahmud, X. Wu, J. L. Sanders, A. Ö. Biliroglu, O. J. Adelegan, I. G. Newsome, F. Y. Yamaner, P. A. Dayton, and Ö. Oralkan, "An improved CMUT structure enabling release and collapse of the plate in the same Tx/Rx cycle for dual-frequency acoustic angiography," *IEEE Trans. Ultrason., Ferroelectr., Freq. Control*, vol. 67, no. 11, pp. 2291–2302, Nov. 2020.

[79] M. M. Mahmud, O. J. Adelegan, J. L. Sanders, X. Zhang, F. Y. Yamaner, P. A. Dayton, and Ö. Oralkan, "Improved CMUT structure and method of operation for dual-frequency acoustic angiography," in *Proc. IEEE Int. Ultrason. Symp. (IUS)*, Sep. 2017, pp. 1–4.

[80] E. Belekov, K. J. Bautista, M. Annayev, O. J. Adelegan, A. O. Biliroglu, T. M. Kierski, J. L. Sanders, R. E. Kemal, E. Sennik, F. Y. Yamaner, P. A. Dayton, and O. Oralkan, "Performance assessment of ultra-wideband and dual-mode 1D CMUT arrays for acoustic angiography," in *Proc. IEEE Int. Ultrason. Symp. (IUS)*, Oct. 2022, pp. 1–4.

[81] Z. M. Hijazi, K. Shivkumar, and D. J. Sahn, "Intracardiac echocardiography during interventional and electrophysiological cardiac catheterization," *Circulation*, vol. 119, no. 4, pp. 587–596, Feb. 2009.

[82] J. Lim, C. Tekes, E. F. Arkan, A. Rezvanitabar, F. L. Degertekin, and M. Ghovanloo, "Highly integrated guidewire ultrasound imaging system-on-a-chip," *IEEE J. Solid-State Circuits*, vol. 55, no. 5, pp. 1310–1323, May 2020.

[83] R. P. Zangabad, J. G. Bosch, F. Mastik, R. H. S. H. Beurskens, V. A. Henneken, J. W. Weekamp, A. F. W. Van Der Steen, and G. Van Soest, "Real-time coded excitation imaging using a CMUT-based side looking array for intravascular ultrasound," *IEEE Trans. Ultrason., Ferroelectr., Freq. Control*, vol. 68, no. 6, pp. 2048–2058, Jun. 2021.

[84] G. Jung, A. Pirouz, C. Tekes, T. Carpenter, M. W. Rashid, A. Revanitabar, D. Cowell, S. Freear, M. Ghovanloo, and F. L. Degertekin, "Single-chip reduced-wire CMUT-on-CMOS system for intracardiac echocardiography," in *Proc. IEEE Int. Ultrason. Symp. (IUS)*, Oct. 2018, pp. 1–4.

[85] S. A. Mirbozorgi, C. Tekes, A. Pirouz, O. Kocaturk, R. Lederman, M. Ghovanloo, and F. L. Degertekin, "A feasibility study for MRI guided CMUT-based intracardiac echocardiography catheters," in *Proc. IEEE Int. Ultrason. Symp. (IUS)*, Sep. 2017, pp. 1–4.

[86] J. Lee, K.-R. Lee, B. E. Eovino, J. H. Park, L. Lin, H.-J. Yoo, and J. Yoo, "A 5.37 mW/Channel pitch-matched ultrasound ASIC with dynamic-bit-shared SAR ADC and 13.2 V charge-recycling TX in standard CMOS for intracardiac echocardiography," in *IEEE Int. Solid-State Circuits Conf. (ISSCC) Dig. Tech. Papers*, Feb. 2019, pp. 190–192.

[87] T. Matéo, N. Sénégond, C. Meynier, D. Gross, P. Vince, M. Tan, E. Kang, and M. Pertijs, "A 1-D CMUT transducer with front-end ASIC in a 9 French catheter for intracardiac echocardiography: Acoustic and imaging evaluation," in *Proc. IEEE Int. Ultrason. Symp. (IUS)*, Sep. 2020, pp. 1–8.

[88] R. Stoute, M. C. Louwerse, V. A. Henneken, and R. Dekker, "Intravascular ultrasound at the tip of a guidewire: Concept and first assembly steps," *Proc. Eng.*, vol. 168, pp. 1563–1567, Jan. 2016.

[89] J. Lim, C. Tekes, F. L. Degertekin, and M. Ghovanloo, "Towards a reduced-wire interface for CMUT-based intravascular ultrasound imaging systems," *IEEE Trans. Biomed. Circuits Syst.*, vol. 11, no. 2, pp. 400–410, Apr. 2017.

[90] Y. Pei, Y. Zhang, S. Hu, Z. Wang, Y. Li, C. He, S. Zhang, R. Wang, W. Zhang, and G. Zhang, "Breast transmission ultrasound tomography based on capacitive micromachined ultrasonic transducer linear arrays," *IEEE Sensors J.*, vol. 22, no. 2, pp. 1209–1217, Jan. 2022.

[91] H. Wang, Y. Ma, H. Yang, H. Jiang, Y. Ding, and H. Xie, "MEMS ultrasound transducers for endoscopic photoacoustic imaging applications," *Micromachines*, vol. 11, no. 10, p. 928, Oct. 2020.

[92] A. Dangi, K. Roy, S. Agrawal, H. Chen, A. Ashok, C. Wible, M. Osman, R. Pratap, and S.-R. Kothapalli, "A modular approach to neonatal whole-brain photoacoustic imaging," *Proc. SPIE*, vol. 11240, Apr. 2020, Art. no. 1124057.

[93] R. K. W. Chee, P. Zhang, M. Maadi, and R. J. Zemp, "Multifrequency interlaced CMUTs for photoacoustic imaging," *IEEE Trans. Ultrason., Ferroelectr., Freq. Control*, vol. 64, no. 2, pp. 391–401, Feb. 2017.

[94] R. Manwar, K. Kratkiewicz, and K. Avanaki, "Overview of ultrasound detection technologies for photoacoustic imaging," *Micromachines*, vol. 11, no. 7, p. 692, Jul. 2020.

[95] S. Paul, A. Thomas, and S. S. Mayanglambam, "Improvement of delay and sum beamforming photoacoustic imaging based on delay-multiply-sum-to-standard-deviation-factor," *Proc. SPIE*, vol. 11642, Aug. 2021, Art. no. 116423.

[96] S. Mulani, S. Paul, M. K. A. Singh, and M. S. Singh, "Improvement of LED-based photoacoustic imaging using sign coherence factor based on lag-delay-multiply-and-sum beamformer," *Proc. SPIE*, vol. 11960, Jan. 2022, Art. no. 119600.

[97] A. Paramanick, K. Roy, D. Samanta, A. K. S. R. Pratap, and M. S. Singh, "Image quality enhancement of PMUT-based photoacoustic imaging," *Proc. SPIE*, vol. 12379, Dec. 2023, Art. no. 123791.

[98] H. Wang, H. Yang, Z. Chen, Q. Zheng, H. Jiang, P. X.-L. Feng, and H. Xie, "Development of dual-frequency PMUT arrays based on thin ceramic PZT for endoscopic photoacoustic imaging," *J. Microelectromech. Syst.*, vol. 30, no. 5, pp. 770–782, Oct. 2021.

[99] H. Wang, H. Yang, H. Jiang, Z. Chen, P. X.-L. Feng, and H. Xie, "A multi-frequency pMUT array based on ceramic PZT for endoscopic photoacoustic imaging," in *Proc. 21st Int. Conf. Solid-State Sensors, Actuators Microsyst.*, Jun. 2021, pp. 30–33.

[100] J. Cai, Y. Wang, L. Lou, S. Zhang, Y. Gu, F. Gao, and T. Wu, "Photoacoustic and ultrosound dual-modality endoscopic imaging based on ALN pmut array," in *Proc. IEEE 35th Int. Conf. Micro Electro Mech. Syst. Conf. (MEMS)*, Jan. 2022, pp. 412–415.

[101] A. Dangi, C. Y. Cheng, S. Agrawal, S. Tiwari, G. R. Datta, R. R. Benoit, R. Pratap, S. Trolier-Mckinstry, and S.-R. Kothapalli, "A photoacoustic imaging device using piezoelectric micromachined ultrasound transducers (PMUTs)," *IEEE Trans. Ultrason., Ferroelectr., Freq. Control*, vol. 67, no. 4, pp. 801–809, Apr. 2020.

[102] J. Chan, Z. Zheng, K. Bell, M. Le, P. H. Reza, and J. T. W. Yeow, "Photoacoustic imaging with capacitive micromachined ultrasound transducers: Principles and developments," *Sensors*, vol. 19, no. 16, p. 3617, Aug. 2019.

[103] R. K. W. Chee, A. Sampaleanu, D. Rishi, and R. J. Zemp, "Top orthogonal to bottom electrode (TOBE) 2-D CMUT arrays for 3-D photoacoustic imaging," *IEEE Trans. Ultrason., Ferroelectr., Freq. Control*, vol. 61, no. 8, pp. 1393–1395, Aug. 2014.

[104] Z. Li, A. K. Ilkhechi, and R. Zemp, "Transparent capacitive micromachined ultrasonic transducers (CMUTs) for photoacoustic applications," *Opt. Exp.*, vol. 27, no. 9, pp. 13204–13218, 2019.

[105] X. Cheng, J. Chen, and C. Li, "A miniature capacitive micromachined ultrasonic transducer array for minimally invasive photoacoustic imaging," *J. Microelectromech. Syst.*, vol. 19, no. 4, pp. 1002–1011, Aug. 2010.

[106] A. Nikoozadeh, C. Chang, J. W. Choe, A. Bhuyan, B. C. Lee, A. Moini, and P. T. Khuri-Yakub, "An integrated ring CMUT array for endoscopic ultrasound and photoacoustic imaging," in *Proc. IEEE Int. Ultrason. Symp. (IUS)*, Jul. 2013, pp. 1178–1181.

[107] L. Peralta, A. Gomez, Y. Luan, B.-H. Kim, J. V. Hajnal, and R. J. Eckersley, "Coherent multi-transducer ultrasound imaging," *IEEE Trans. Ultrason., Ferroelectr., Freq. Control*, vol. 66, no. 8, pp. 1316–1330, Aug. 2019, doi: 10.1109/TUFFC.2019.2921103.

[108] A. Gholampour, J.-W. Müller, C. Cano, M. R. H. M. van Sambeek, R. Lopata, H.-M. Schwab, and M. Wu, "Multiperspective photoacoustic imaging using spatially diverse CMUTs," *IEEE Trans. Ultrason., Ferroelectr., Freq. Control*, vol. 70, no. 1, pp. 16–24, Jan. 2023.

[109] C. Seok, O. Adelegan, A. O. Biliroglu, F. Y. Yamaner, and Ö. Oralkan, "A 2D ultrasonic transmit phased array based on a 32x32 CMUT array flip-chip bonded to an ASIC for neural stimulation," in *Proc. IEEE Int. Ultrason. Symp. (IUS)*, Sep. 2020, pp. 1–4.

[110] C. Seok, X. Wu, F. Y. Yamaner, and Ö. Oralkan, "A front-end integrated circuit for a 2D capacitive micromachined ultrasound transducer (CMUT) array as a noninvasive neural stimulator," in *Proc. IEEE Int. Ultrason. Symp. (IUS)*, Sep. 2017, pp. 1–4.

[111] C. Seok, F. Y. Yamaner, M. Sahin, and Ö. Oralkan, "A wearable ultrasonic neurostimulator—Part I: A 1D CMUT phased array system for chronic implantation in small animals," *IEEE Trans. Biomed. Circuits Syst.*, vol. 15, no. 4, pp. 692–704, Aug. 2021.

[112] C. Seok, O. J. Adelegan, A. Ö. Biliroglu, F. Y. Yamaner, and Ö. Oralkan, "A wearable ultrasonic neurostimulator—Part II: A 2D CMUT phased array system with a flip-chip bonded ASIC," *IEEE Trans. Biomed. Circuits Syst.*, vol. 15, no. 4, pp. 705–718, Aug. 2021.

[113] R. M. Jones, C. F. Caskey, P. A. Dayton, Ö. Oralkan, and G. F. Pinton, "Transcranial neuromodulation array with imaging aperture for simultaneous multifocus stimulation in nonhuman primates," *IEEE Trans. Ultrason., Ferroelectr., Freq. Control*, vol. 69, no. 1, pp. 261–272, Jan. 2022.

[114] S. Kawasaki, V. Giagka, M. de Haas, M. Louwerse, V. Henneken, C. van Heesch, and R. Dekker, "Pressure measurement of geometrically curved ultrasound transducer array for spatially specific stimulation of the vagus nerve," in *Proc. 9th Int. IEEE/EMBS Conf. Neural Eng. (NER)*, San Francisco, CA, USA, Mar. 2019, pp. 1239–1242.

[115] S. Kawasaki, E. Dijkema, M. Saccher, V. Giagka, J. J. H. B. Schleipen, and R. Dekker, "Schlieren visualization of focused ultrasound beam steering for spatially specific stimulation of the vagus nerve," in *Proc. 10th Int. IEEE/EMBS Conf. Neural Eng. (NER)*, May 2021, pp. 1113–1116.

[116] A. I. Velea, J. Wilson, A. Gollhardt, C. B. Karuthedath, A. S. Thanniyil, and V. Giagka, "Non-monolithic fabrication of thin-film microelectrode arrays on PMUT transducers as a bimodal neuroscientific investigation tool*," in *Proc. 45th Annu. Int. Conf. IEEE Eng. Med. Biol. Soc. (EMBC)*, Jul. 2023, pp. 1–12.

[117] V. Cotero, Y. Fan, T. Tsaava, A. M. Kressel, I. Hancu, P. Fitzgerald, K. Wallace, S. Kaanumalle, J. Graf, W. Rigby, T.-J. Kao, J. Roberts, C. Bhushan, S. Joel, T. R. Coleman, S. Zanos, K. J. Tracey, J. Ashe, S. S. Chavan, and C. Puleo, "Noninvasive sub-organ ultrasound stimulation for targeted neuromodulation," *Nature Commun.*, vol. 10, no. 1, pp. 1–15, Mar. 2019.

[118] V. Cotero, H. Miwa, J. Graf, J. Ashe, E. Loghin, D. Di Carlo, and C. Puleo, "Peripheral focused ultrasound neuromodulation (pFUS)," *J. Neurosci. Methods*, vol. 341, Jul. 2020, Art. no. 108721, doi: 10.1016/j.jneumeth.2020.108721.

[119] D. P. Zachs, S. J. Offutt, R. S. Graham, Y. Kim, J. Mueller, J. L. Auger, N. J. Schuldt, C. R. Kaiser, A. P. Heiller, R. Dutta, H. Guo, J. K. Alford, B. A. Binstadt, and H. H. Lim, "Noninvasive ultrasound stimulation of the spleen to treat inflammatory arthritis," *Nature Commun.*, vol. 10, no. 1, pp. 1–20, Dec. 2019.

[120] M. E. Downs, S. A. Lee, G. Yang, S. Kim, Q. Wang, and E. E. Konofagou, "Non-invasive peripheral nerve stimulation via focused ultrasound in vivo," *Phys. Med. Biol.*, vol. 63, no. 3, Jan. 2018, Art. no. 035011, doi: 10.1088/1361-6560/aa9fc2.

[121] T. Costa, C. Shi, K. Tien, J. Elloian, F. A. Cardoso, and K. L. Shepard, "An integrated 2D ultrasound phased array transmitter in CMOS with pixel pitch-matched beamforming," *IEEE Trans. Biomed. Circuits Syst.*, vol. 15, no. 4, pp. 731–742, Aug. 2021.

[122] H. Rivandi and T. L. Costa, "A 2D ultrasound phased-array transmitter ASIC for high-frequency U.S. stimulation and powering," *IEEE Trans. Biomed. Circuits Syst.*, vol. 17, no. 4, pp. 701–712, Jul. 2023.

[123] C. R. Bawiec, W. A. N'Djin, G. Bouchoux, N. Sénégond, N. Guillen, and J.-Y. Chapelon, "Preliminary investigation of dual mode CMUT probe for ultrasound image guided HIFU therapy," in *Proc. IEEE Int. Ultrason. Symp. (IUS)*, Sep. 2017, pp. 1–4.

[124] J. H. Jang, C. Chang, M. F. Rasmussen, A. Moini, K. Brenner, D. N. Stephens, Ö. Oralkan, and B. Khuri-Yakub, "Integration of a dual-mode catheter for ultrasound image guidance and HIFU ablation using a 2-D CMUT array," in *Proc. IEEE Int. Ultrason. Symp. (IUS)*, Sep. 2017, pp. 1–4.

[125] O. Farhanieh, A. Sahafi, R. B. Roy, A. S. Ergun, and A. Bozkurt, "Integrated HIFU drive system on a chip for CMUT-based catheter ablation system," *IEEE Trans. Biomed. Circuits Syst.*, vol. 11, no. 3, pp. 534–546, Jun. 2017.

[126] H.-S. Yoon, C. Chang, J. H. Jang, A. Bhuyan, J. W. Choe, A. Nikoozadeh, R. D. Watkins, D. N. Stephens, K. Butts Pauly, and B. T. Khuri-Yakub, "Ex vivo HIFU experiments using a 32 × 32-element CMUT array," *IEEE Trans. Ultrason., Ferroelectr., Freq. Control*, vol. 63, no. 12, pp. 2150–2158, Dec. 2016.

[127] W. A. N'Djin, B. Gerold, J. Vion-Bailly, M. S. Canney, A. Nguyen-Dinh, A. Carpentier, and J.-Y. Chapelon, "Capacitive micromachined ultrasound transducers for interstitial high-intensity ultrasound therapies," *IEEE Trans. Ultrason., Ferroelectr., Freq. Control*, vol. 64, no. 8, pp. 1245–1260, Aug. 2017.

[128] C. R. Bawiec, W. A. N'Djin, G. Bouchoux, N. Sénégond, N. Guillen, and J.-Y. Chapelon, "Preliminary investigation of a 64-element capacitive micromachined ultrasound transducer (CMUT) annular array designed for high intensity focused ultrasound (HIFU)," *IRBM*, vol. 39, no. 5, pp. 295–306, Nov. 2018.

[129] C. Shi, V. Andino-Pavlovsky, S. A. Lee, T. Costa, J. Elloian, E. E. Konofagou, and K. L. Shepard, "Application of a sub-0.1-mm^3 implantable mote for in vivo real-time wireless temperature sensing," *Sci. Adv.*, vol. 7, no. 19, May 2021, doi: 10.1126/sciadv.abf6312.

[130] M. D. Menz, P. Ye, K. Firouzi, A. Nikoozadeh, K. B. Pauly, P. Khuri-Yakub, and S. A. Baccus, "Radiation force as a physical mechanism for ultrasonic neurostimulation of the ex vivo retina," *J. Neurosci.*, vol. 39, no. 32, pp. 6251–6264, Aug. 2019, doi: 10.1523/JNEUROSCI.2394-18.2019.

[131] C. van Damme, G. K. Wardhana, A. I. Velea, V. Giagka, and T. L. Costa, "A high-frequency flexible ultrasonic cuff implant for high-precision vagus nerve ultrasound neuromodulation," 2023, *arXiv:2311.12034*.

[132] C. Shi, T. Costa, J. Elloian, Y. Zhang, and K. L. Shepard, "A 0.065-mm^3 monolithically-integrated ultrasonic wireless sensing mote for real-time physiological temperature monitoring," *IEEE Trans. Biomed. Circuits Syst.*, vol. 14, no. 3, pp. 412–424, Jun. 2020.

[133] C. Shi, T. Costa, J. Elloian, and K. L. Shepard, "Monolithic integration of micron-scale piezoelectric materials with CMOS for biomedical applications," in *IEDM Tech. Dig.*, Mar. 2018, pp. 4.5.1–4.5.4.

[134] G. K. Wardhana, M. Mastrangeli, and T. L. Costa, "Maximization of transmitted acoustic intensity from silicon integrated piezoelectric ultrasound transducers," in *Proc. IEEE Int. Ultrason. Symp. (IUS)*, Oct. 2022, pp. 1–4.

[135] E. S. Young, F. Yalcin Yamaner, and Ö. Oralkan, "Ultrasound-based post-endovascular aneurysm repair (EVAR) monitoring device," in *Proc. IEEE Int. Ultrason. Symp. (IUS)*, Oct. 2019, pp. 1948–1950.

[136] M. Saccher, S. Kawasaki, and R. Dekker, "The long-term reliability of pre-charged CMUTs for the powering of deep implanted devices," in *Proc. IEEE Int. Ultrason. Symp. (IUS)*, Sep. 2021, pp. 1–4.

[137] H. Basaeri, Y. Yu, D. Young, and S. Roundy, "A MEMS-scale ultrasonic power receiver for biomedical implants," *IEEE Sensors Lett.*, vol. 3, no. 4, pp. 1–4, Apr. 2019.

[138] F. Pop, S. D. Calisgan, B. Herrera, A. Risso, S. Kang, V. Rajaram, Z. Qian, and M. Rinaldi, "Zero-power ultrasonic wakeup receiver based on MEMS switches for implantable medical devices," *IEEE Trans. Electron Devices*, vol. 69, no. 3, pp. 1327–1332, Mar. 2022.

[139] M. Saccher, S. S. Lolla, S. Kawasaki, and R. Dekker, "Time-efficient low power time/phase-reversal beamforming for the tracking of ultrasound implantable devices," in *Proc. IEEE Int. Ultrason. Symp. (IUS)*, Oct. 2022, pp. 1–4.

[140] H. Ding, S. Akhbari, B. E. Eovino, Y. Wu, J. Xie, and L. Lin, "Ultrasonic imaging of muscle-like phantoms using bimorph pmuts toward wearable muscle disorder diagnostics," in *Proc. IEEE Micro Electro Mech. Syst. (MEMS)*, 2018, pp. 396–399.

[141] L. Jia, L. Shi, C. Sun, S. Liu, and G. Wu, "Aln based piezoelectric micromachined ultrasonic transducers for continuous monitoring of the mechano-acoustic cardiopulmonary signals," in *Proc. IEEE 34th Int. Conf. Micro Electro Mech. Syst. (MEMS)*, Jan. 2021, pp. 426–429.

[142] H. Ding, D. Yang, M. Qu, C. Yang, X. Chen, X. Le, K. Zhu, J. Xu, L. Lin, and J. Xie, "A pulsed wave Doppler ultrasound blood flowmeter by PMUTs," *J. Microelectromech. Syst.*, vol. 30, no. 5, pp. 680–682, Oct. 2021.

[143] X. Ding, Z. Wu, M. Gao, M. Chen, J. Li, T. Wu, and L. Lou, "A high-sensitivity bowel sound electronic monitor based on piezoelectric micromachined ultrasonic transducers," *Micromachines*, vol. 13, no. 12, p. 2221, Dec. 2022.

[144] K. Roy, K. Kalyan, A. Ashok, V. Shastri, A. A. Jeyaseelan, A. Mandal, and R. Pratap, "A PMUT integrated microfluidic system for fluid density sensing," *J. Microelectromech. Syst.*, vol. 30, no. 4, pp. 642–649, Aug. 2021.

[145] O. Z. Olszewski, R. MacLoughlin, A. Blake, M. O'Neill, A. Mathewson, and N. Jackson, "A silicon-based MEMS vibrating mesh nebulizer for inhaled drug delivery," *Proc. Eng.*, vol. 168, pp. 1521–1524, Jan. 2016.

[146] D. Certon, F. Barcella, J. B. Messaoud, J. Ladroue, L. Vecellio, N. Heuze-Vourc'h, and D. Alquier, "Flexible CMUT for vibrating mesh nebulize," in *Proc. IEEE Int. Ultrason. Symp. (IUS)*, Oct. 2019, pp. 742–745.

[147] S. L. Grue, M. Engholm, and E. V. Thomsen, "Electrical insulation of CMUT elements using DREM and lapping," in *Proc. IEEE Int. Ultrason. Symp. (IUS)*, Sep. 2020, pp. 1–4.

[148] D. Certon, S. Audiere, L. Colin, N. Senegond, D. Alquier, J.-M. Gregoire, L. Sandrin, and V. Miette, "CMUT-based single element transducer applied to 1D transient ultrasound elastography," in *Proc. IEEE Int. Ultrason. Symp. (IUS)*, Oct. 2018, pp. 1–4.

ELISABETTA MOISELLO (Member, IEEE) was born in Pavia, Italy, in 1993. She received the master's degree (summa cum laude) in electronic engineering and the Ph.D. degree in microelectronics from the University of Pavia, in 2017 and 2020, respectively. She is currently a Postdoctoral Research Fellow and a Contract Professor with the University of Pavia. Her research interests include sensor interface circuits, switching dc-dc converters, and wireless power transfer. She has been and still is part of the Organizing Committee of the PRIME Conference and has served on the Technical Program Committees of several international conferences, such as PRIME, ICECS, and NEWCAS. She is an Associate Editor of IEEE Transactions on Circuits and Systems—II: Express Briefs.

LARA NOVARESI (Graduate Student Member, IEEE) was born in Pavia, Italy, in 1995. She received the bachelor's and master's degrees (summa cum laude) in electronic engineering from the University of Pavia, in 2017 and 2020, respectively, where she is currently pursuing the Ph.D. degree in microelectronics. Her research interests include sensory interface circuits and ultrasound imaging systems.

ESHANI SARKAR (Graduate Student Member, IEEE) received the B.Sc. and M.Sc. degrees in physics from the University of Calcutta (CU), West Bengal, India, in 2016 and 2019, respectively, and the master's (M.Tech.) degree in nanoscience and engineering from the Indian Institute of Science (IISc), Bengaluru, in 2022. She is currently pursuing the Ph.D. degree with the Department of Microelectronics (Bioelectronics Section), Faculty of Electrical Engineering, Mathematics, and Computer Science (EEMCS), Delft University of Technology (TU, Delft). Her current research interests include piezo-MEMS, ultrasound, transducer design, fabrication, and characterization of biomedical implantable devices for ultrasound neuromodulation.

PIERO MALCOVATI (Senior Member, IEEE) received the degree in electronic engineering from the University of Pavia, Italy, in 1991, and the Ph.D. degree in electrical engineering from ETH Zurich, in 1996. From 1996 to 2001, he was an Assistant Professor with the Department of Electrical, Computer, and Biomedical Engineering, University of Pavia, where he was an Associate Professor, from 2002 to 2017. Since 2017, he has been a Full Professor with the University of Pavia. His research interests include microsensor interface circuits, power electronics circuits, and high-performance data converters. He has been a member of the Technical Program Committee for several international conferences, including ISSCC, ESSCIRC, SENSORS, ICECS, and PRIME. He is an Associate Editor of the IEEE Journal of Solid-State Circuits.

TIAGO L. COSTA (Senior Member, IEEE) received the B.Sc. and M.Sc. degrees in electrical engineering and the Ph.D. degree in electrical and computer engineering from Instituto Superior Técnico (IST), University of Lisbon, Portugal, in 2006, 2008, and 2014, respectively. The Ph.D. thesis focused on the development of CMOS integrated circuits for magnetoresistive sensors interface for biomolecular recognition and neuronal recording. From Summer 2015 to Summer 2019, he was a Postdoctoral Research Associate with the Bioelectronics Systems Laboratory, Columbia University, New York, USA, where he worked on ultrasound phased array systems for noninvasive nerve stimulation. Since October 2019, he has been an Assistant Professor of bioelectronics with the Delft University of Technology, where his group works on the development of ultrasound microsystems for the next generation neurotechnologies. He is an Associate Editor of IEEE Transactions on Biomedical Circuits and Systems.

EDOARDO BONIZZONI (Senior Member, IEEE) was born in Pavia, Italy, in 1977. He received the Laurea degree (summa cum laude) in electronic engineering and the Ph.D. degree in electronic, computer, and electrical engineering from the University of Pavia, Italy, in 2002 and 2006, respectively. Since 2002, he has been with the Department of Electrical, Computer, and Biomedical Engineering, University of Pavia, where he is currently an Associate Professor. His research interests include the design and testing of A/D converters, high-performance analog blocks, sensor interface circuits, and power management solutions. He is a member of the Analog Signal Processing Technical Committee of IEEE CASS. He is a TPC Member of the IEEE Custom Integrated Circuits Conference (CICC). He has served the CAS Society as an Associate Editor of IEEE Transactions on Circuits and Systems—II: Express Briefs, from 2011 to 2015, and IEEE Transactions on Circuits and Systems—I: Regular Papers, from 2016 to 2019. From 2020 to 2021 and from 2022 to 2023, he was an Associate Editor-in-Chief of *Digital Communications* and IEEE Transactions on Circuits and Systems—II: Express Briefs, respectively. Currently, he is an Editor-in-Chief of IEEE Transactions on Circuits and Systems—II: Express Briefs. He has been part of several organizing committees of IEEE CASS Conferences, such as ISCAS, ISICAS, ICECS, MWSCAS, and PRIME.

• • •